

# Geometry-Guided Camera Motion Understanding in VideoLLMs

Haoan Feng<sup>1</sup>, Sri Harsha Musunuri<sup>2</sup>, Guan-Ming Su<sup>2</sup>,  
<sup>1</sup>University of Maryland, College Park, <sup>2</sup>Dolby Laboratories Inc.

## Abstract

*Camera motion is a fundamental geometric signal that shapes visual perception and cinematic style, yet current video-capable vision-language models (VideoLLMs) rarely represent it explicitly and often fail on fine-grained motion primitives. We address this gap with a framework of **benchmarking, diagnosis, and injection**. We curate **CameraMotionDataset**, a large-scale synthetic dataset with explicit camera control, formulate camera motion as constraint-aware multi-label recognition, and construct a VQA benchmark—**CameraMotionVQA**. Across diverse off-the-shelf VideoLLMs, we observe substantial errors in recognizing camera motion primitives. Probing experiments on a Qwen2.5-VL vision encoder suggest that camera motion cues are weakly represented, especially in deeper ViT blocks, helping explain the observed failure modes. To bridge this gap without costly training or fine-tuning, we propose a lightweight, model-agnostic pipeline that extracts geometric camera cues from 3D foundation models (3DFMs), predicts constrained motion primitives with a temporal classifier, and injects them into downstream VideoLLM inference via structured prompting. Experiments demonstrate improved motion recognition and more camera-aware model responses, highlighting geometry-driven cue extraction and structured prompting as practical steps toward a camera-aware VideoLLM and VLA system. Dataset and benchmark will be released upon publication.*

## 1. Introduction

Video-capable vision-language models (VideoLLMs) have improved substantially on high-level video semantics, including recognition of objects, actions, and narrative events across diverse video lengths [26]. However, an essential component of video meaning, especially in edited content such as films, TV series, and online compilations, lies not only in *what* appears in the frames, but also in *how* it is captured. Camera motion (*e.g.*, pan, tilt, and dolly) is a core cinematographic device that guides attention, reveals spatial layout, and communicates the author’s intent [18].

Accordingly, camera motion is both central to film grammar and useful for camera-aware description, layout-oriented retrieval, and spatial reasoning.

Despite its importance, current VideoLLMs remain unreliable in recognizing fine-grained camera-motion primitives. Camera motion is a spatiotemporal geometric signal that is not localized to any single frame, and it is easily confounded by object motion, cuts, and motion blur. Consequently, models with strong frame-level perception may still fail to model the camera as the source of the visual stream. Moreover, as we later show, common VideoLLM pipelines compress visual tokens with network depth, which can attenuate motion-sensitive cues. This gap is unsurprising, as most large-scale video captioning and VQA corpora lack explicit supervision for camera motion.

To study this gap under controlled conditions, we introduce **CameraMotionDataset**, a synthetic dataset of 12k within-shot segments annotated with fine-grained camera-motion labels. A *shot* is a temporally contiguous sequence of frames captured by a single camera without cuts; we focus on non-overlapping 1-second segments within each shot. Each segment is annotated with a set of camera-motion labels drawn from a fixed taxonomy of 15 atomic motions. Built on this dataset, **CameraMotionVQA** provides a multiple-choice benchmark that evaluates open-source VideoLLMs under a standardized VQA protocol.

A central hypothesis of this work is that reliable camera-motion cues can be derived from models with strong geometric and 3D reasoning capabilities *without modifying* the VideoLLM backbone. Specifically, we use a frozen 3D foundation model (VGGT [28]) to extract camera cues, train a lightweight temporal classifier to predict constrained motion primitives, and inject the predictions into downstream VideoLLMs via structured prompting.

Beyond performance gains, we seek to understand *where* camera-motion information is lost in typical VideoLLM pipelines. By probing intermediate vision-encoder features with Q-Former-style query tokens [14], we observe that camera-motion cues become progressively less recoverable from shallow to deeper blocks, consistent with our hypothesis on token compression and the lack of explicit motion

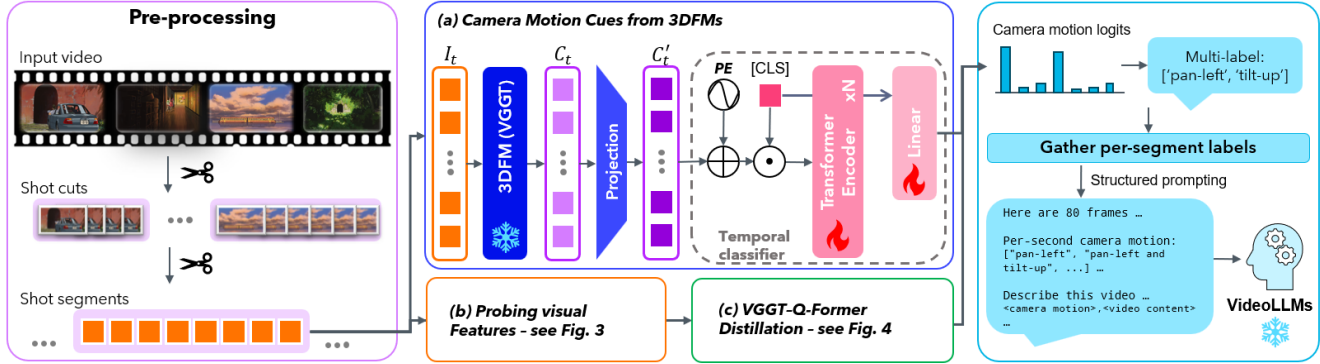


Figure 1. **Overall pipeline.** Camera cues are extracted from a frozen 3DFM (VGGT) and passed to a Transformer-based temporal classifier to predict camera-motion primitives, and per-second motions are injected as a structured prompt field for VideoLLMs without modifying VideoLLM weights. For clarity, the probing and distillation pipelines are shown separately in Fig. 3 and Fig. 4.

supervision. These findings motivate the use of geometry-derived camera cues from 3DFMs as an external, plug-in signal. Our contributions are threefold:

- **CameraMotionDataset and CameraMotionVQA.** We introduce a synthetic, shot-consistent dataset with fine-grained camera-motion labels and a multiple-choice VQA benchmark for evaluating open-source VideoLLMs.
- **Camera-cue assisted motion recognition and structured prompting.** We propose a model-agnostic pipeline that extracts camera cues from a frozen 3DFM (VGGT), predicts motion primitives with a lightweight temporal classifier, and injects them into frozen VideoLLM inference via structured prompting (Fig. 1).
- **Probing-based diagnosis.** We analyze where and why camera-motion cues are lost in VideoLLM vision encoders, helping explain failure modes on CameraMotion-VQA and motivating our geometry-aware cue injection.

## 2. Related Work

### 2.1. Camera motion in cinematic video understanding

Cinematography depends on both *what* is shown and *how* it is filmed (camera, framing, composition). Recent benchmarks therefore evaluate film-grammar attributes beyond generic video QA [27, 30]. CameraBench [18] defines a cinematographer-informed motion taxonomy and evaluates shot-aligned clips, revealing confusions between extrinsic motion (e.g., dolly) and intrinsic change (e.g., zoom). Complementary benchmarks expand to multi-attribute cinematography understanding: CineTechBench [30] and ShotBench [19] cover frame-wise cinematic attributes with expert annotations and provide VQA-style protocols, while VidComposition [27] emphasizes compiled-video settings in which cinematographic understanding remains challenging for multimodal large language models (MLLMs). Shot-by-Shot [32] shows shot-level film-grammar cues can steer description generation via prompting, without retraining.

Existing datasets span settings from per-frame cinematic attributes to geometry-grounded supervision. CineScale [23], CineScale2 [24], MovieShots [22], Full-Shots [16], and HistShot [12] provide cinematic priors, but not geometry-consistent motion primitives at short-segment granularity. Newer datasets provide explicit 3D signals: SpatialVID [29] offers per-frame depth and pose-derived motion instructions, while OmniTr [34] encodes motion as parameterized programs linking language to trajectories.

Camera motion is also a primary control signal in video generation. Recent models [1, 2, 10, 11, 20, 21, 35] condition diffusion/video-to-video generation on explicit trajectories, camera/ray embeddings, or geometry renders, or transfer motion from a reference video. Particularly, ReCamMaster [2] releases *MultiCamVideo*, which we use to derive our dataset and benchmark. Although these works target controllable *generation*, their motion parameterizations also motivate the design of reliable *recognition* models of fine-grained primitives under compositional and exclusivity constraints [11].

### 2.2. Vision-language models and VideoLLMs

VideoLLMs extend image VLMs to video by encoding sampled frames, compressing visual tokens, and conditioning an LLM for instruction following, captioning, and QA. This “frame aggregation + LLM reasoning” paradigm captures high-level semantics, but token compression can attenuate subtle temporal cues, including camera motion.

Open-source VideoLLMs can be organized by their temporal design and videoLLM interface. Strong-backbone models (e.g., Qwen2.5-VL [3] and InternVL [4]) strengthen the vision tower and time/position encoding to better support long-context video. Connector-based models [15, 33, 39] keep the LLM mostly fixed and add lightweight temporal modules with aggressive token reduction to fit multi-frame inputs. Instruction-tuned assistants [5, 37] emphasize curated video-instruction data and post-training to improve temporal reasoning without major architectural changes.

Video-native systems [13, 31, 36] use stronger video encoders and/or video-centric pretraining to improve spatiotemporal representations.

Bridging modules offer a parameter-efficient way to integrate video into LLMs. Query bottlenecks (*e.g.*, Q-Former) summarize frame features into a small set of query tokens, improving efficiency over dense patch tokens [14, 38]. However, cinematography-centric benchmarks still show weak fine-grained camera-motion recognition, suggesting recent progress is driven more by sampling, grounding, and alignment than explicit camera-motion representation.

### 2.3. 3D foundation models and geometric cues for VideoLLMs

3D foundation models (3DFMs) are pretrained models that learn transferable 3D representations and infer geometric attributes (*e.g.*, dense structure) from visual input. As a representative, VGGT [28] is a feed-forward geometry transformer that jointly predicts camera parameters, depth/point maps, and tracking cues from one or multiple views, exposing camera-aware tokens as geometric cues. Follow-up work improves efficiency [25], and learning-based SfM systems amortize reconstruction to enhance robustness [6, 7], expanding practical sources of camera geometry.

Recent work connects geometric priors to vision-language reasoning by adding explicit geometry branches [40] or distilling signals from frozen 3DFMs into compact tokens consumable by VideoLLMs without altering their input modality [9, 17]. This motivates using off-the-shelf 3DFM cues as a model-agnostic source of camera-aware signals for VideoLLMs.

**Summary.** Benchmarks position camera motion at the intersection of geometry and semantics: although datasets provide explicit trajectories, VideoLLMs struggle to recover fine-grained motion primitives. We therefore leverage off-the-shelf 3DFMs to extract camera cues, predict constraint-consistent motion labels, and inject them into frozen VideoLLMs via structured prompting. Our probing and distillation experiments further clarify when geometric cues can be extracted and incorporated efficiently.

## 3. Method

### 3.1. Problem overview

Our goal is to provide *generic-video* camera motion understanding for VideoLLMs. Given an input video, we first split it into shots using an off-the-shelf shot segmentation module (*e.g.*, Shot-by-Shot [32]). Each shot is split into non-overlapping 1-second segments uniformly sampled. The goal is to predict a constrained combination of camera motion primitives. We denote the target camera motion of a segment by a multi-hot vector  $\mathbf{y} \in \{0, 1\}^K$  over  $K=15$  atomic primitives, where multiple primitives may

co-occur (*e.g.*, pan-left + tilt-up) but mutually exclusive pairs (*e.g.*, pan-left vs. pan-right) are forbidden.

Our camera motion module is lightweight and plug-and-play: we extract explicit camera cues from a frozen 3D foundation model (3DFM), predict motion primitives using a lightweight temporal classifier, and inject the resulting per-second motion sequence into a structured prompt for downstream VideoLLMs. In this work, VGGT is chosen because it produces per-frame *camera tokens* in a single forward pass; these tokens implicitly encode rich camera geometry cues (pose and dynamics) in a unified per-scene coordinate system, which we find are typically not well-preserved by VideoLLM vision features. Pipeline overview and its integration with prompting is shown in Fig. 1.

### 3.2. CameraMotionDataset construction and CameraMotionVQA benchmark

We build a labeled camera-motion dataset from the *Multi-CamVideo* dataset introduced in ReCamMaster [2]. Multi-CamVideo contains photorealistic dynamic scenes rendered in Unreal Engine 5 [8], with dense frame-wise camera calibration (intrinsic) and camera poses (extrinsic). It covers 13.6K dynamic scenes and includes 136K videos with 112K distinct camera trajectories; videos are rendered at 15 fps, and trajectories are explicit camera extrinsic sequences.

As shown in Fig. 2, each video is divided into non-overlapping 1-second segments to ensure camera motion labels are accurately aligned with actual camera changes. For each segment, we uniformly sample  $T=8$  frames and resize to  $336 \times 336$ , which provides a favorable accuracy-efficiency trade-off for camera motion recognition.

**Camera motion label from extrinsic params.** We assign camera motion labels by analyzing frame-wise camera extrinsic matrices, following the taxonomy and operational definitions in CameraBench [18]. Concretely, we compute per-segment translation and rotation changes (*e.g.*, yaw/pitch/roll deltas and forward/backward translation) and map them to motion primitives (*e.g.*, pan-left, tilt-down, dolly-in) using thresholded pattern matching in pose dynamics. Compound motions are produced when multiple primitives are detected simultaneously (*e.g.*, arc-clockwise, dolly-in). With precisely controlled camera motion, our labeling approach provides sufficiently accurate annotation results for each segment. To validate label quality, we conduct a human verification study on 720 randomly selected segments and observe 93% agreement.

We further observe substantial class imbalance. Thus, we apply stratified sampling to construct a balanced subset while preserving diversity across atomic and compound-motion classes, yielding 12,274 segments in total. For *CameraMotionDataset*, a standard train/val/test split is created by 80%/10%/10% folds. Camera motion taxonomy and labeling procedure, and dataset re-balancing details are pro-

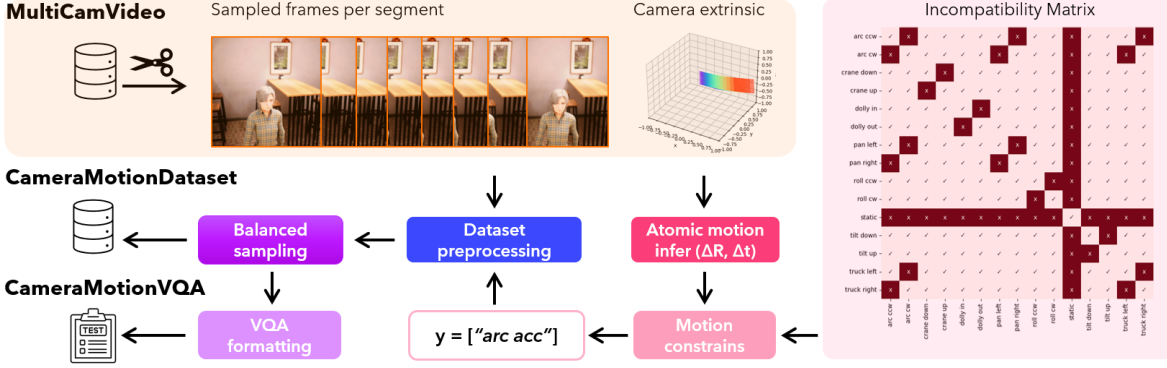


Figure 2. **Flow chart for dataset/benchmark construction.** From MultiCamVideo [2], video clips and camera extrinsics are preprocessed (split, resized, and normalized) and labeled with several motion constraints (e.g., incompatibility). A subset of shot segments is sampled based on motion primitives to balance classes, before storing as CameraMotionDataset and formulated into CameraMotionVQA records.

vided in the supplementary.

### Atomic primitives, constraints, and canonicalization.

We define 15 atomic primitives and represent each segment label as a multi-hot vector. To enforce physically and semantically valid combinations, we define a symmetric incompatibility matrix  $\mathbf{M} \in \{0, 1\}^{K \times K}$ , where  $\mathbf{M}_{ij} = 1$  indicates that primitives  $i$  and  $j$  cannot co-occur (see Fig. 2). Label-set canonicalization limits the maximum number of primitives, uses deterministic ordering and de-duplication, for consistent evaluation and prompt serialization.

**CameraMotionVQA benchmark.** To benchmark off-the-shelf VideoLLMs under a unified protocol, we construct a multiple-choice VQA benchmark, named CameraMotionVQA. Each question corresponds to a 1-second clip and provides four candidate answers: one ground-truth motion label set and three *distractors*. Distractors are sampled to have similar label complexity as the ground-truth (number of primitives), avoiding trivial answer-length bias. In addition, all candidates are valid under the incompatibility constraints. VQA templates are included in the supplementary.

Table 1 positions our dataset and benchmark against existing cinematic benchmarks and video datasets. Based on this comparison, we argue that it is necessary to create a camera motion-focused dataset with trustworthy labels derived deterministically from extrinsic params and sufficient scale to train a robust modern classifier.

### 3.3. Camera motion cues from 3DFMs

Camera motion is fundamentally geometric, arising from coherent changes in camera pose over time. Although modern VideoLLMs are trained for semantic alignment and temporal coherence, geometric camera-motion cues are not reliably preserved in their intermediate vision representations (Sec. 3.6). To compensate for this missing geometric signal, we use a 3DFM as an external camera motion cue extractor.

Our framework is agnostic to the specific 3DFM: any model that can provide per-frame camera descriptors (e.g., pose-related tokens or camera parameter estimates) can be

plugged into our pipeline. VGGT [28] produces camera tokens in a single forward pass and has been shown to encode camera pose and motion dynamics. Given a 1-second segment with  $T$  sampled frames, we run VGGT on each frame and obtain a camera token sequence  $\{\mathbf{c}_t\}_{t=1}^T$ , where  $\mathbf{c}_t \in \mathbb{R}^{2048}$ . These camera tokens serve as the input to our temporal classifier, as shown in Fig. 1.

### 3.4. Constraint-regularized motion classifier

We train a lightweight classifier to map camera tokens  $\mathbf{c}_t$  to constrained multi-label camera-motion predictions. A linear projection  $\mathbf{W}_p$  is applied to form an information bottleneck: VGGT tokens may encode rich camera-related factors, and the projection stabilizes training by distilling the subset most relevant to motion prediction. Then, add a sinusoidal positional encoding and prepend a learnable [CLS] token. The resulting sequence is processed by an  $L$ -layer Transformer encoder, and logits are predicted from the final [CLS] token (i.e.,  $\mathbf{Z}_L[0, :]$ ) by a linear projection  $\mathbf{W}_o$ :

$$\mathbf{z}_t = \text{PE}(\mathbf{W}_p \mathbf{c}_t), \quad t = 1, \dots, T, \quad (1)$$

$$\mathbf{Z}_0 = [\mathbf{z}_{\text{cls}}, \mathbf{z}_1, \dots, \mathbf{z}_T], \quad (2)$$

$$\mathbf{Z}_L = \text{TransformerEnc}(\mathbf{Z}_0), \quad (3)$$

$$\mathbf{s} = \mathbf{W}_o \mathbf{Z}_L[0, :] + \mathbf{b}_o, \quad (4)$$

where  $\mathbf{s} \in \mathbb{R}^K$  are the output logits and  $p_k = \text{sigmoid}(s_k)$  denote per-class probability. Following the constrained multi-label formulation in Sec. 3.1, we optimize a binary cross-entropy loss with two regularizations:

$$\mathcal{L}_{\text{bce}} = - \sum_{k=1}^K \left( y_k \log p_k + (1 - y_k) \log(1 - p_k) \right), \quad (5)$$

$$\mathcal{L}_{\text{inc}} = \sum_{1 \leq i < j \leq K} \mathbf{M}_{ij} p_i p_j, \quad (6)$$

$$\mathcal{L}_{\text{card}} = \max \left( 0, 1 - \sum_{k=1}^K p_k \right)^2 + \max \left( 0, \sum_{k=1}^K p_k - 3 \right)^2 \quad (7)$$

Table 1. **Positioning of our datasets against prior benchmarks and datasets.** “Motion-level” indicates the granularity of camera supervision (primitive vs. composition of motions). Our CameraMotionDataset provides constrained primitive-level supervision with explicit synthetic camera parameters, while CameraMotionVQA converts the same 1s within-shot segments into a multiple-choice evaluation protocol. A full comparison with detailed annotation structure and intended usage is provided in the supplementary material.

	Motion-level	Granularity	Temporal unit	QA protocol	Intended use	Camera params
CameraBench [18]	Primitive	Multi-label	Short clips	Caption, Yes/No QA	Benchmark + fine-tune	No
CineTechBench [30]	Composition	Coarse	Frames / short clips	Caption, MCQ	Benchmark	No
VidComposition [27]	Composition	Coarse	Compiled videos	MCQ	Benchmark	No
CineScale2 [24]	-	-	Frames	No	Training dataset	No
<b>CameraMotionDataset</b>	<b>Primitive</b>	<b>Multi-label</b>	<b>1s within-shot</b>	No	<b>Training dataset</b>	<b>Yes</b>
<b>CameraMotionVQA</b>	<b>Primitive</b>	<b>Multi-label</b>	<b>1s within-shot</b>	<b>MCQ</b>	<b>Benchmark</b>	No

where  $\lambda_{inc}$  and  $\lambda_{card}$  control the strengths of incompatibility and cardinality regularization. In our implementation, we use  $\lambda_{inc} = 1.0$  and  $\lambda_{card} = 1.0$  by default.

At inference, we threshold probabilities at  $\tau=0.5$  and enforce constraints by removing mutually exclusive primitives within each primitive group and applying canonicalization.

### 3.5. Motion injection via structured prompting

As a training and fine-tuning free approach, camera motion cues are injected via structured prompting, leaving VideoLLM weights unchanged. For a shot consisting of  $S$  one-second segments, each motion label is predicted and serialized as a short string (e.g., `static` or `pan-left` and `tilt-up`), and these strings are concatenated into a per-shot list: Per-second camera motion:  $[m_1, m_2, \dots, m_S]$ . We prepend this motion list to the user instruction to provide an explicit temporal scaffold. Empirically, this conditioning might improve the temporal grounding of generated descriptions and reduce camera-motion hallucinations, as the model can align content changes with the provided motion sequence (Fig. 7). Our final prompt template is:

```
Here are [N] consecutive video frames.
They are evenly sampled at a frame rate
of [r] FPS.
Per-second camera motion: [m1,m2,...].
Describe this video using the filmmaker's
language, highlighting lighting, framing,
composition, and especially camera usage
that connects different frames.
For example: "At the beginning, <video
content>; then <camera motion>, <video
content>; ...; finally, <camera motion>,
<video content>."
```

### 3.6. Probing motion sensitivity via Q-Former

Q-Former [14] style probing provides an effective “read-out” mechanism: a small set of learnable query tokens can extract task-relevant information from high-dimensional frozen visual tokens via cross-attention, enabling a parameter-efficient diagnostic of what information is present in the representation. As shown in Fig. 3, we probe on Qwen2.5-VL [3], whose vision encoder is a dynamic-resolution ViT with window attention blocks

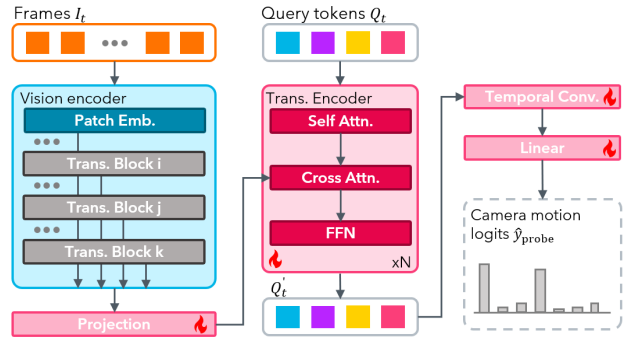


Figure 3. **Probing experiment schematic.** Query tokens  $Q_t$  gather camera motion-related information from the projected intermediate visual features of the frozen vision encoder. Camera motion logits are predicted from the temporal convolution output of the transferred vision tokens  $Q'_t$ .

and periodic full-attention blocks at indices  $\{7, 15, 23, 31\}$ . Thus, we extract visual tokens from patch embedding and the full-attention blocks. This pipeline consists of: (i) a linear projection that bottlenecks the frozen visual tokens to the query dimension; (ii) 4 learnable query tokens processed by 2 Transformer Encoders; (iii) a 1D temporal convolution over the query tokens to produce a single classification token; and (iv) a linear classifier to predict multi-label logits. The probe is trained with the same loss in Sec. 3.4.

### 3.7. VGGT-Q-Former distillation

VGGT provides high-quality camera tokens but is computationally heavy (1.2B params). As shown in Fig. 4, to reduce inference cost, we propose to distill VGGT’s camera perception by a lightweight Q-Former-based student. Specially, the student follows the same *interleaved local- and global-attention* as VGGT for camera reasoning, enabling temporally grounded yet context-aware representations.

**Q-Former with interleaved local-frame and global attention.** We assign one learnable query token to each (temporally indexed) feature map and have processing blocks that alternate between local (frame) attention and global attention. In local attention, each query attends only to the visual tokens of its assigned frame, encouraging temporally grounded camera cues. In global attention, all queries at-

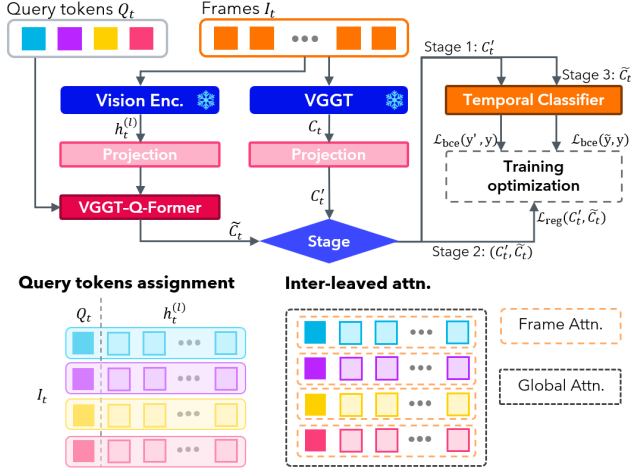


Figure 4. **VGGT-Q-Former schematic.** Camera tokens and visual tokens are both bottlenecked by a projection layer. Query tokens gather camera motion-related information via interleaved local-/global-attention blocks and regress the projected camera tokens to distill the camera perception capability of VGGT. Branch annotated with Stage  $i$  indicating different training optimization objectives and flows of tokens.

tend jointly across frames, enabling cross-frame aggregation of camera dynamics. As in VGGT, query tokens  $Q_t$  have 256 dimensions, and the outputs from the final local and global blocks are concatenated to form the final distillation result  $\tilde{c}_t$  of dim 512.

**Three-stage progressive training.** As illustrated in Fig. 4, a progressive training strategy is adopted: (1) train the motion classifier on projected VGGT tokens; (2) train the distiller (VGGT-Q-Former) by regressing the projected VGGT tokens using mean squared error; and (3) jointly fine-tune the VGGT-Q-Former and classifier. The regression loss is

$$\mathcal{L}_{\text{reg}} = \sum_{t=1}^T |\tilde{c}_t - c'_t|_2^2, \quad (8)$$

where  $c'_t$  denotes the projected VGGT token and  $\tilde{c}_t$  denotes the distilled token.

At inference, VGGT is replaced by VGGT-Q-Former, and the same temporal motion classifier is used to get labels for each segment. In Sec. 4.5, we report the trade-off between efficiency and accuracy of this distillation approach.

## 4. Experiments

### 4.1. Experimental setup

All experiments are conducted on a single NVIDIA RTX A6000 GPU. We evaluate camera-motion recognition on **CameraMotionDataset** and **CameraMotionVQA** as detailed in Sec. 3.2. CameraMotionVQA formats each segment as a 4-way multiple-choice question, and models are evaluated using answer accuracy. For evaluating the camera motion multi-label task, we report **instance accuracy**

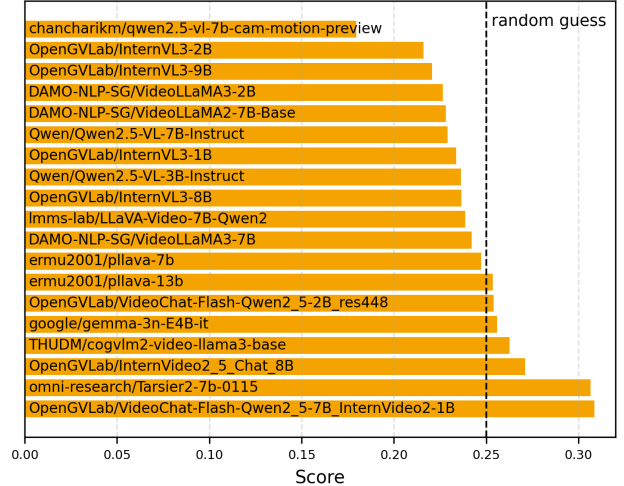


Figure 5. **Off-the-shelf VideoLLM performance on CameraMotionVQA.** Horizontal bars report overall multiple-choice accuracy. All models, labeled by their Hugging Face model names, use an identical frame input and VQA prompt template.

(exact match of all labels), **Macro-F1** across motion primitives, and **Weighted-F1** weighted by label frequency.

### 4.2. How well do off-the-shelf VideoLLMs recognize camera motion?

As described in Sec. 3.2, we evaluate diverse off-the-shelf VideoLLMs under the unified CameraMotionVQA protocol. Figure 5 shows that most models perform near the random-guess rate (25%), revealing a substantial *camera-motion blindness* gap. Notably, a structured fine-tuning baseline from CameraBench [18] performs worse than its off-the-shelf counterpart (Qwen2.5-VL). Qualitatively, models frequently confuse geometrically similar primitives (e.g., truck vs. pan) and produce inconsistent directional predictions (e.g., pan-left vs. pan-right) in the presence of salient object motion.

We attribute this gap to the lack of explicit camera-motion supervision in VideoLLM training data, where representations are optimized for semantic alignment and temporal reasoning rather than precise 3D geometric change. Our probing results (Sec. 4.4) support this claim and motivate injecting explicit geometric camera cues.

### 4.3. Camera motion recognition from 3D foundation-model cues

We run a frozen 3D foundation model (VGGT) on  $\{I_t\}_{t=1}^8$  and extract per-frame camera cues (camera tokens  $C_t \in \mathbb{R}^{2048}$ ). A lightweight temporal classifier (Sec. 3.4) consumes the cue sequence and predicts constrained multi-label motions. Unless otherwise stated, VGGT is frozen, and we train a shallow Transformer classifier with 4 encoder blocks and 8 attention heads. Each camera token is projected to  $C'_t \in \mathbb{R}^{512}$ ; a learnable [CLS] token is prepended;

Table 2. **Multi-label camera-motion recognition results on the test split of CameraMotionDataset.** *Inst. Acc.*: exact multi-label matching accuracy; *Macro-F1*: class-averaged F1 score; *Weighted-F1*: sample frequency-weighted F1 score.

Method	Inst. Acc.↑	Macro-F1↑	Weighted-F1↑
VGGT w. constraints	<b>0.738</b>	<b>0.87</b>	<b>0.92</b>
VGGT w/o. constraints	0.572	0.79	0.84
VGGT-Q-Former	0.638	0.83	0.87
Q-Former probing	0.450	0.69	0.74

the final [CLS] embedding is mapped to  $K$  logits. In the supplementary, we ablate the number of encoder blocks, attention heads, and hidden size, and find that the current setting achieves a favorable accuracy–compute trade-off.

Table 2 shows that VGGT-derived cues with a lightweight classifier substantially outperform off-the-shelf VideoLLM baselines (Fig. 5). Removing constraint enforcement (*VGGT w/o. constraints*) reduces instance-level accuracy, indicating that modeling axis-wise mutual exclusion improves performance even with strong cues. Per-label prediction results (in the supplementary) show that errors concentrate on rare or ambiguous primitives, consistent with the long-tail distribution. We also observe unreliable predictions for the *static* class, which is likely out-of-distribution for VGGT, whose reconstruction prior assumes camera motion. Static segments may require dedicated handling beyond 3DFM priors.

Despite its effectiveness, VGGT cue extraction is costly: the 1.2B-parameter model performs multi-view 3D reasoning over all frames, dominating latency and memory.

#### 4.4. Probing motion sensitivity in a vision encoder

As described in Sec. 3.6, we freeze the Qwen2.5-VL vision encoder and train a small Q-Former-style probe on intermediate features to predict motion labels. This pathway is used *solely* to diagnose representation bottlenecks. The probe comprises 2 Transformer blocks with 8 heads and 4 learnable query tokens. Query tokens and projected features are 768-dimensional.

As shown in Fig. 6, performance peaks at the first full-attention block and declines in later layers. This suggests that camera-motion information is weakly encoded and becomes less accessible as features are optimized for semantic alignment with the language model. Replacing temporal convolution with average pooling further reduces accuracy, indicating that explicit temporal modeling is necessary to derive camera motion from token sequences.

#### 4.5. Distilling 3D Camera Cues for efficiency

VGGT-based cue extraction is computationally expensive at inference: the 1.2B-parameter backbone performs multi-view 3D reasoning over all frames. To reduce cost, we distill teacher camera tokens into a compact student Q-

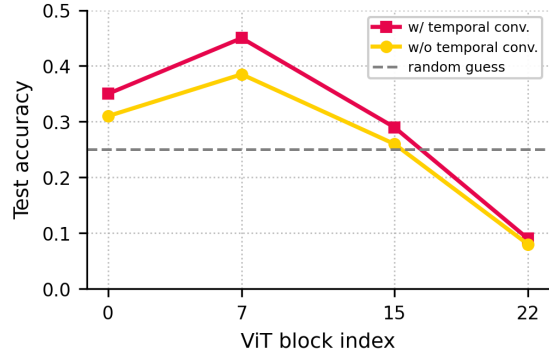


Figure 6. **Results of probing experiment.** Intermediate features from the frozen vision tower at different Transformer block indices are probed by query tokens. Performance peaks at a shallow intermediate block and degrades in later layers, suggesting that camera-motion cues are not reliably preserved.

Table 3. **Efficiency comparison of camera-motion recognition pipelines.** We compare trainable parameter count, peak GPU memory, and inference time throughput for: the full VGGT-based classifier; the distilled VGGT-Q-Former pipeline; and the Q-Former probing experiment. All measurements are conducted on an RTX A6000 with batch size 16 and input resolution  $336 \times 336$ .

Pipeline	Params (M)	Peak mem. (MBs)	Throughput (samples/s)
VGGT classifier	9.47	23649.11	4.39
VGGT-Q-Former	9.15	9202.63	23.36
Q-Former probing	15.18	9232.23	25.12

Former (VGGT-Q-Former) that reuses frozen VideoLLM vision features (Sec. 3.7). We use hidden features  $h_t^l$  from the 7th block of Qwen2.5-VL, where probing shows higher camera-motion recoverability (Fig. 6). The student attends to visual tokens and predicts embeddings that regress projected teacher tokens. We use 4 learnable queries (one per frame group) and follow VGGT’s interleaved local/global attention (Fig. 4): 2 local blocks (query–frame) and 2 global blocks (cross-frame). Training proceeds in three stages: (1) train the motion classifier for 50 epochs; (2) train query tokens for 100 epochs to regress teacher tokens; (3) jointly fine-tune the student and classifier for 30 epochs. We use Adam with a learning rate of  $1e-4$ .

Table 3 reports inference overhead. Although instance accuracy drops by 8.13%, distillation substantially reduces end-to-end cost. The distilled model (8.72M vs. 1.2B) achieves  $5.3\times$  throughput at 39% peak memory, offering a favorable accuracy–latency trade-off. Overall, teacher cues maximize accuracy but are costly, whereas distilled cues improve efficiency at some loss in accuracy.

#### 4.6. Qualitative results for structured prompting

Our goal is to enable VideoLLMs to produce camera-aware, filmmaker-style descriptions that capture *what* happens and

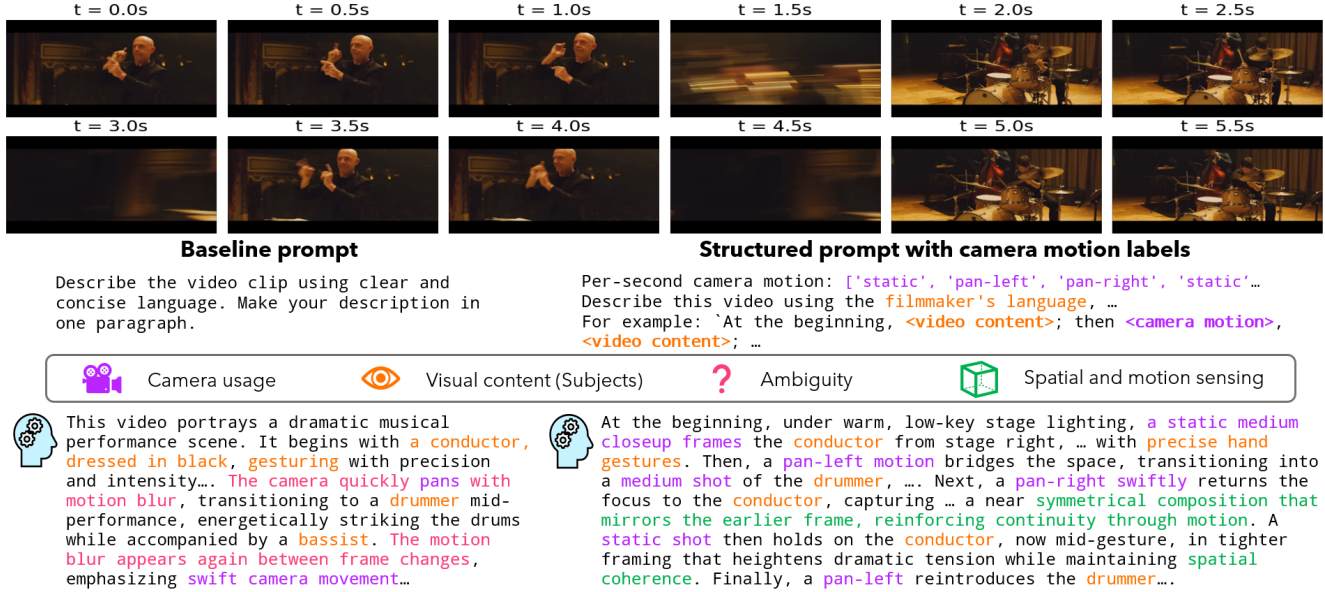


Figure 7. **Structured motion header enables camera-aware and temporally grounded descriptions.** Top: a 5-second clip sampled at 2 fps. Bottom: outputs from the same VideoLLM with different prompts. The baseline description correctly identifies subjects but produces **ambiguous motion statements**, without specifying **direction or temporal structure**. With structured motion cues, the model generates explicit **camera usage**, maintains **subject focus**, and introduces **spatial-temporal reasoning such as continuity and coherence**.

how the shot is filmed and evolves over time. Following Sec. 3.5, we prepend a per-second motion header to the prompt without modifying model weights. Figure 7 shows a representative example. Under the baseline prompt, the model recognizes the conductor and drummer, but describes motion vaguely (e.g., “camera quickly pans with motion blur”) without direction or temporal structure. The description mixes possible cuts and camera movement, leading to ambiguity in how frames are connected.

In contrast, with the provided explicit motion cues, the same VideoLLM produces a temporally structured narrative. It explicitly grounds motion direction (pan-left and pan-right), describes framing (static medium close-up), and adds spatial reasoning (e.g., “mirrors the earlier frame”, “spatial coherence”). This suggests motion headers improve motion correctness and encourage geometry-aware, temporally consistent reasoning.

Beyond motion correctness, the header biases the model toward spatial and motion reasoning. The structured cues promote continuity, geometric consistency, and frame-to-frame transitions, reducing generic descriptions. This suggests that camera motion labels act as geometric priors that steer large VideoLLMs toward more temporally grounded and cinematographically aware reasoning. Full outputs and other examples are provided in the supplementary.

## 5. Conclusion and Discussion

Camera motion is a fundamental geometric signal that shapes video perception, yet it is rarely modeled explicitly

in current VideoLLMs. In this work, this gap is addressed through a loop of *benchmarking*, *diagnosis*, and *injection*: we introduce a shot-consistent 1-second dataset and a VQA benchmark that formulates fine-grained motion primitives as a constrained multi-label recognition task; we show via probing that camera motion cues are only weakly recoverable from frozen VideoLLM vision features; and we propose a lightweight pipeline that extracts cues from a frozen 3D foundation model (VGGT). The pipeline predicts constrained motion primitives and injects them via structured prompting *without updating VLM weights*.

Camera cues support applications where *how* a scene is filmed matters in addition to *what*, including descriptive video services (DVS) [32], media recommendation and retrieval by filmmaking metadata [24], camera-aware video attribute or authorship analysis [16], and plagiarism detection. More broadly, our results suggest camera awareness remains a structured supervision problem and there is representation gap in current VideoLLMs. In this work, we propose a plug-and-play solution, in which synthetic camera-controlled data provides scalable supervision, 3DFMs inject geometric priors, and distillation offers a favorable cost-performance trade-off. Limitations include the synthetic-to-real gap, focus on camera *extrinsic* rather than *intrinsic* changes (e.g., zoom), and only a single 3DFM backbone is explored. Future work will extend to broader camera configurations and 3DFMs, and systematically study how camera cues transfer to downstream video understanding and generation tasks.

## References

- [1] Sherwin Bahmani, Ivan Skorokhodov, Guocheng Qian, Aliaksandr Siarohin, Willi Menapace, Andrea Tagliasacchi, David B Lindell, and Sergey Tulyakov. Ac3d: Analyzing and improving 3d camera control in video diffusion transformers. In *Proceedings of the Computer Vision and Pattern Recognition Conference*, pages 22875–22889, 2025. 2
- [2] Jianhong Bai, Menghan Xia, Xiao Fu, Xintao Wang, Lianrui Mu, Jinwen Cao, Zuozhu Liu, Haoji Hu, Xiang Bai, Pengfei Wan, et al. Recammaster: Camera-controlled generative rendering from a single video. *arXiv preprint arXiv:2503.11647*, 2025. 2, 3, 4
- [3] Shuai Bai, Keqin Chen, Xuejing Liu, Jialin Wang, Wenbin Ge, Sibao Song, Kai Dang, Peng Wang, Shijie Wang, Jun Tang, et al. Qwen2. 5-vl technical report. *arXiv preprint arXiv:2502.13923*, 2025. 2, 5
- [4] Zhe Chen, Jiannan Wu, Wenhai Wang, Weijie Su, Guo Chen, Sen Xing, Muyan Zhong, Qinglong Zhang, Xizhou Zhu, Lewei Lu, et al. Internvl: Scaling up vision foundation models and aligning for generic visual-linguistic tasks. In *CVPR*, pages 24185–24198, 2024. 2
- [5] Zesen Cheng, Sicong Leng, Hang Zhang, Yifei Xin, Xin Li, Guanzheng Chen, Yongxin Zhu, Wenqi Zhang, Ziyang Luo, Deli Zhao, et al. Videollama 2: Advancing spatial-temporal modeling and audio understanding in video-llms. *arXiv preprint arXiv:2406.07476*, 2024. 2
- [6] Andrea Porfiri Dal Cin, Georgi Dikov, Jihong Ju, and Mohsen Ghafoorian. Anymap: Learning a general camera model for structure-from-motion with unknown distortion in dynamic scenes. In *Proceedings of the Computer Vision and Pattern Recognition Conference*, pages 16674–16684, 2025. 3
- [7] Sven Elfle, Qunjie Zhou, and Laura Leal-Taixé. Light3r-sfm: Towards feed-forward structure-from-motion. In *Proceedings of the IEEE/CVF Conference on Computer Vision and Pattern Recognition*, pages 16774–16784, 2025. 3
- [8] Epic Games. Unreal engine 5. 3
- [9] Minghao Guo, Meng Cao, Jiachen Tao, Rongtao Xu, Yan Yan, Xiaodan Liang, Ivan Laptev, and Xiaojun Chang. Glad: Geometric latent distillation for vision-language-action models. *arXiv preprint arXiv:2512.09619*, 2025. 3
- [10] Hao He, Yinghao Xu, Yuwei Guo, Gordon Wetzstein, Bo Dai, Hongsheng Li, and Ceyuan Yang. Cameractrl: Enabling camera control for text-to-video generation. *arXiv preprint arXiv:2404.02101*, 2024. 2
- [11] Hao He, Ceyuan Yang, Shanchuan Lin, Yinghao Xu, Meng Wei, Liangke Gui, Qi Zhao, Gordon Wetzstein, Lu Jiang, and Hongsheng Li. Cameractrl ii: Dynamic scene exploration via camera-controlled video diffusion models. In *Proceedings of the IEEE/CVF International Conference on Computer Vision*, pages 13416–13426, 2025. 2
- [12] Daniel Helm, Florian Kleber, and Martin Kampel. Histshot: A shot type dataset based on historical documentation during wwii. In *ICPRAM*, pages 636–643, 2022. 2
- [13] Wenyi Hong, Weihang Wang, Ming Ding, Wenmeng Yu, Qingsong Lv, Yan Wang, Yean Cheng, Shiyu Huang, Junhui Ji, Zhao Xue, et al. Cogvlm2: Visual language models for image and video understanding. *arXiv preprint arXiv:2408.16500*, 2024. 3
- [14] Junnan Li, Dongxu Li, Silvio Savarese, and Steven Hoi. Blip-2: Bootstrapping language-image pre-training with frozen image encoders and large language models. pages 19730–19742. PMLR, 2023. 1, 3, 5
- [15] Xinhao Li, Yi Wang, Jiashuo Yu, Xiangyu Zeng, Yuhang Zhu, Haian Huang, Jianfei Gao, Kunchang Li, Yan He, Chenting Wang, et al. Videochat-flash: Hierarchical compression for long-context video modeling. *arXiv preprint arXiv:2501.00574*, 2024. 2
- [16] Yuzhi Li, Tianfeng Lu, and Feng Tian. A lightweight weak semantic framework for cinematographic shot classification. *Scientific Reports*, 13(1):16089, 2023. 2, 8
- [17] Yifan Li, Zhixin Lai, Wentao Bao, Zhen Tan, Anh Dao, Kewei Sui, Jiayi Shen, Dong Liu, Huan Liu, and Yu Kong. Visual large language models for generalized and specialized applications. *arXiv preprint arXiv:2501.02765*, 2025. 3
- [18] Zhiqiu Lin, Siyuan Cen, Daniel Jiang, Jay Karhade, Hwei Wang, Charanik Mitra, Tiffany Ling, Yuhang Huang, Sifan Liu, Mingyu Chen, et al. Towards understanding camera motions in any video. *arXiv preprint arXiv:2504.15376*, 2025. 1, 2, 3, 5, 6
- [19] Hongbo Liu, Jingwen He, Yi Jin, Dian Zheng, Yuhao Dong, Fan Zhang, Ziqi Huang, Yanan He, Yangguang Li, Weichao Chen, et al. Shotbench: Expert-level cinematic understanding in vision-language models. *arXiv preprint arXiv:2506.21356*, 2025. 2
- [20] Yiwen Liu, Jianguo Jiang, Min Yu, Boquan Li, Myung Hwan Na, and Gang Li. Posemaster: Editing your pose in a video with a one-shot framework. In *International Conference on Advanced Data Mining and Applications*, pages 239–253. Springer, 2025. 2
- [21] Yawen Luo, Xiaoyu Shi, Jianhong Bai, Menghan Xia, Tianfan Xue, Xintao Wang, Pengfei Wan, Di Zhang, and Kun Gai. Camclonemaster: Enabling reference-based camera control for video generation. In *Pro-*

- ceedings of the SIGGRAPH Asia 2025 Conference Papers*, pages 1–10, 2025. 2
- [22] Anyi Rao, Jiaze Wang, Linning Xu, Xuekun Jiang, Qingqiu Huang, Bolei Zhou, and Dahua Lin. A unified framework for shot type classification based on subject centric lens. In *European Conference on Computer Vision*, pages 17–34. Springer, 2020. 2
- [23] Mattia Savardi, András Bálint Kovács, Alberto Signoroni, and Sergio Benini. Cinescale: A dataset of cinematic shot scale in movies. *Data in Brief*, 36: 107002, 2021. 2
- [24] Mattia Savardi, András Bálint Kovács, Alberto Signoroni, and Sergio Benini. Cinescale2: a dataset of cinematic camera features in movies. *Data in Brief*, 51:109627, 2023. 2, 5, 8
- [25] Zhijian Shu, Cheng Lin, Tao Xie, Wei Yin, Ben Li, Zhiyuan Pu, Weize Li, Yao Yao, Xun Cao, Xiaoyang Guo, et al. Litevggt: Boosting vanilla vggg via geometry-aware cached token merging. *arXiv preprint arXiv:2512.04939*, 2025. 3
- [26] Yunlong Tang, Jing Bi, Siting Xu, Luchuan Song, Susan Liang, Teng Wang, Daoan Zhang, Jie An, Jingyang Lin, Rongyi Zhu, et al. Video understanding with large language models: A survey. *IEEE TCSVT*, 2025. 1
- [27] Yunlong Tang, Junjia Guo, Hang Hua, Susan Liang, Mingqian Feng, Xinyang Li, Rui Mao, Chao Huang, Jing Bi, Zeliang Zhang, et al. Vidcomposition: Can mllms analyze compositions in compiled videos? In *CVPR*, pages 8490–8500, 2025. 2, 5
- [28] Jianyuan Wang, Minghao Chen, Nikita Karaev, Andrea Vedaldi, Christian Rupprecht, and David Novotny. Vggt: Visual geometry grounded transformer. In *CVPR*, pages 5294–5306, 2025. 1, 3, 4
- [29] Jiahao Wang, Yufeng Yuan, Rujie Zheng, Youtian Lin, Jian Gao, Lin-Zhuo Chen, Yajie Bao, Yi Zhang, Chang Zeng, Yanxi Zhou, et al. Spatialvid: A large-scale video dataset with spatial annotations. *arXiv preprint arXiv:2509.09676*, 2025. 2
- [30] Xinran Wang, Songyu Xu, Xiangxuan Shan, Yuxuan Zhang, Muxi Diao, Xueyan Duan, Yanhua Huang, Kongming Liang, and Zhanyu Ma. Cinetech-bench: A benchmark for cinematographic technique understanding and generation. *arXiv preprint arXiv:2505.15145*, 2025. 2, 5
- [31] Yi Wang, Kunchang Li, Xinhao Li, Jiashuo Yu, Yinan He, Guo Chen, Baoqi Pei, Rongkun Zheng, Zun Wang, Yansong Shi, et al. Internvideo2: Scaling foundation models for multimodal video understanding. In *ECCV*, pages 396–416. Springer, 2024. 3
- [32] Junyu Xie, Tengda Han, Max Bain, Arsha Nagrani, Eshika Khandelwal, Gül Varol, Weidi Xie, and Andrew Zisserman. Shot-by-shot: Film-grammar-aware training-free audio description generation. *arXiv preprint arXiv:2504.01020*, 2025. 2, 3, 8
- [33] Lin Xu, Yilin Zhao, Daquan Zhou, Zhijie Lin, See Kiong Ng, and Jiashi Feng. Pllava: Parameter-free llava extension from images to videos for video dense captioning. *arXiv preprint arXiv:2404.16994*, 2024. 2
- [34] Xiaoda Yang, Jiayang Xu, Kaixuan Luan, Xinyu Zhan, Hongshun Qiu, Shijun Shi, Hao Li, Shuai Yang, Li Zhang, Checheng Yu, et al. Omnicam: Unified multimodal video generation via camera control. *arXiv preprint arXiv:2504.02312*, 2025. 2
- [35] Mark Yu, Wenbo Hu, Jinbo Xing, and Ying Shan. Trajectorycrafter: Redirecting camera trajectory for monocular videos via diffusion models. In *Proceedings of the IEEE/CVF international conference on computer vision*, pages 100–111, 2025. 2
- [36] Liping Yuan, Jiawei Wang, Haomiao Sun, Yuchen Zhang, and Yuan Lin. Tarsier2: Advancing large vision-language models from detailed video description to comprehensive video understanding. *arXiv preprint arXiv:2501.07888*, 2025. 3
- [37] Boqiang Zhang, Kehan Li, Zesen Cheng, Zhiqiang Hu, Yuqian Yuan, Guanzheng Chen, Sicong Leng, Yuming Jiang, Hang Zhang, Xin Li, et al. Video-ollama 3: Frontier multimodal foundation models for image and video understanding. *arXiv preprint arXiv:2501.13106*, 2025. 2
- [38] Hang Zhang, Xin Li, and Lidong Bing. Video-llama: An instruction-tuned audio-visual language model for video understanding. In *Proceedings of the 2023 conference on empirical methods in natural language processing: system demonstrations*, pages 543–553, 2023. 3
- [39] Yuanhan Zhang, Jinming Wu, Wei Li, Bo Li, Zejun Ma, Ziwei Liu, and Chunyuan Li. Llava-video: Video instruction tuning with synthetic data. *arXiv preprint arXiv:2410.02713*, 2024. 2
- [40] Duo Zheng, Shijia Huang, Yanyang Li, and Liwei Wang. Learning from videos for 3d world: Enhancing mllms with 3d vision geometry priors. *arXiv preprint arXiv:2505.24625*, 2025. 3

# Geometry-Guided Camera Motion Understanding in VideoLLMs - Supplementary Material

## Contents

<b>A Camera Motion Taxonomy and Constraints</b>	<b>1</b>
A.1 Atomic Motion Primitives	1
A.2 Incompatibility constraints and label-set canonicalization	2
<b>B Dataset Construction Details</b>	<b>2</b>
B.1 Pose-to-label mapping	2
B.2 Re-balancing and class distribution	4
<b>C CameraMotionVQA Protocol</b>	<b>4</b>
C.1 Prompt templates and answer normalization	4
C.2 Distractor sampling algorithm	4
<b>D Additional Experimental Results</b>	<b>5</b>
D.1 Classifier capacity ablation	5
D.2 Per-label breakdown and confusion analysis	6
<b>E Full Prompts and additional Qualitative Examples</b>	<b>7</b>
E.1 Full prompt templates	7
E.2 More qualitative examples	8

## A. Camera Motion Taxonomy and Constraints

We adopt the camera motion taxonomy proposed in CameraBench [1] and refer readers to that work for a comprehensive definition of motion primitives, annotation guidelines, and constraint design. CameraBench formalizes camera motion as a set of atomic cinematographic operations (*e.g.*, pan, tilt, dolly, roll, arc) with clear geometric interpretation and explicit rules to avoid contradictory labels.

In this work, we use a controlled subset of 15 primitives tailored to short (1-second) within-shot segments, focusing on the extrinsic parameter changes of the camera. Specifically, we focus on principal rotation and translation operations that can be reliably identified at this temporal granularity, while preserving the incompatibility structure defined in CameraBench (*e.g.*, opposing directions along the same degree of freedom are mutually exclusive, and `static` cannot co-occur with any non-static motion).

Our taxonomy is therefore not a redefinition, but a task-specific instantiation of the CameraBench framework, designed to support constrained multi-label benchmarking and

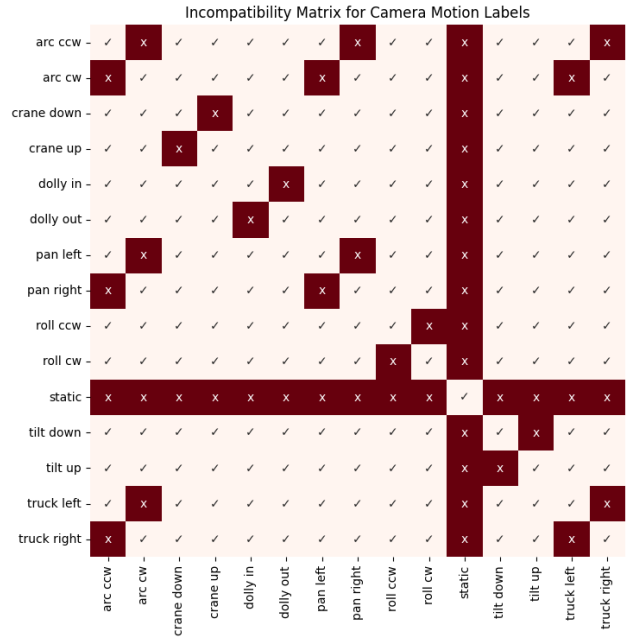


Figure 1. **Incompatibility matrix for constrained multi-label camera motion.** Entry  $M_{ij}=1$  indicates that primitives  $i$  and  $j$  are mutually exclusive and cannot co-occur in the same 1-second segment. The axis structure produces block-wise exclusivity (*e.g.*, left/right pairs), and `static` is incompatible with all non-static primitives. Row/column ordering matches the primitive index order used in our dataset and experiments.

systematic diagnosis of camera motion recognition in VideoLLMs.

### A.1. Atomic Motion Primitives

Our benchmark instantiates a compact, implementation-friendly subset of  $K=15$  atomic motion primitives, summarized in Tab. 1. Each primitive corresponds to a distinct geometric degree of freedom of the camera motion: three rotations (yaw, pitch, roll), three translations (X, Y, Z), a coupled rotation–translation pattern (`arc`), and a `static` state. This axis-aligned parameterization keeps the label space interpretable, physically grounded, and directly compatible with 3D camera representations.

The primitives are designed to be identifiable at the 1-second, within-shot granularity used in our benchmark, and they follow standard cinematographic terminology. Across different axes, primitives may co-occur (e.g., `pan left + tilt up`, or `dolly in + pan right`), motivating a multi-label rather than single-label formulation. We also include `arc` to capture common cinematographic motion where yaw rotation is coupled with lateral translation, which is difficult to describe as a single pure-axis primitive. Finally, `static` denotes the absence of dominant camera motion above predefined thresholds and serves as a diagnostic case for distinguishing true camera motion from object-induced or scene-induced apparent motion in VideoLLMs.

## A.2. Incompatibility constraints and label-set canonicalization

Camera motion primitives are not independent. We enforce geometric exclusivity constraints using a symmetric incompatibility matrix  $\mathbf{M} \in \{0, 1\}^{K \times K}$ , where  $\mathbf{M}_{ij}=1$  indicates that primitives  $i$  and  $j$  cannot co-occur in the same 1-second segment. Figure 1 visualizes  $\mathbf{M}$ ; the row/column ordering matches the primitive index ordering used throughout the dataset, training, and evaluation. Within each degree of freedom, opposing directions are mutually exclusive (e.g., `pan left` vs. `pan right`), and `static` is mutually exclusive with any non-static primitive. These constraints prevent contradictory supervision and yield a well-defined target space for constrained multi-label recognition (and the corresponding VQA-style evaluation).

To make labels deterministic and comparable across data generation, training logs, and evaluation scripts, we canonicalize each segment’s label set as follows: (i) remove duplicates; (ii) drop any label set that violates  $\mathbf{M}$  (i.e., contains a conflicting pair); (iii) sort remaining labels by a fixed global order (the primitive index order used in Fig. 1); and (iv) enforce the cardinality of at least one and at most three primitives per segment. The last step reflects our benchmark design assumption that 1-second clips rarely contain more than three dominant, distinguishable camera motions, and it ensures a bounded and interpretable output space for both classifiers and VideoLLM prompting.

## B. Dataset Construction Details

We construct **CameraMotionDataset** and **CameraMotionVQA** to provide controlled, geometry-aware supervision and standardized evaluation for camera motion understanding in VideoLLMs. As summarized in Tab. 2, existing benchmarks primarily focus on broad cinematographic techniques, perceptual composition attributes, or real-world camera motion without explicit geometric supervision. In contrast, our dataset is built from synthetic videos with known camera parameters, segmented into fixed 1-second within-shot clips, and annotated with constrained multi-

label motion primitives. As shown in the main paper, this design enables (i) precise primitive-level supervision, (ii) constraint-consistent evaluation via a multiple-choice VQA protocol, and (iii) controlled studies of geometry-derived camera cues and motion-token distillation. Below, we detail the data source, segmentation strategy, label generation process, and balancing procedure.

### B.1. Pose-to-label mapping

Each 1-second segment contains  $T=15$  camera extrinsics  $\{\mathbf{E}_t\}_{t=1}^T$ , where  $\mathbf{E}_t = [\mathbf{R}_t \mid \mathbf{t}_t] \in \mathbb{R}^{3 \times 4}$ . Translations are expressed in world units (meters in the renderer), and rotations are represented as  $3 \times 3$  matrices. We assume a right-handed coordinate system where the camera forward axis corresponds to the negative  $x$ -axis, and yaw rotation occurs about the world vertical axis.

The pose sequence is mapped to primitive labels using two signals: (i) net translation expressed in the initial camera frame and (ii) accumulated inter-frame rotation. All angles are computed in degrees, and Algorithm 1 summarizes the full procedure.

**Rotation statistics.** For consecutive frames, we compute the relative rotation  $\mathbf{R}_{\Delta,t} = \mathbf{R}_t \mathbf{R}_{t-1}^\top$  and convert it to an axis-angle representation. We accumulate signed changes for yaw (pan), pitch (tilt, estimated from the forward-vector change), and roll. Let  $\Delta_{\text{pan}}, \Delta_{\text{tilt}}, \Delta_{\text{roll}}$  denote the total signed changes over the segment, and  $\Sigma_{\text{pan}}, \Sigma_{\text{tilt}}, \Sigma_{\text{roll}}$  denote the accumulated absolute changes.

**Static / rotation-dominant case.** Let  $d_{\text{trans}}$  be the total translation distance (sum of inter-frame translations). If  $d_{\text{trans}} < 0.05$ , we treat the segment as rotation-dominant. We then assign `static` if  $\Sigma_{\text{pan}} < 0.2$  and  $\Sigma_{\text{tilt}} < 0.2$ ; otherwise we assign `pan left/right` based on the sign of  $\Delta_{\text{pan}}$  when  $\Sigma_{\text{pan}} > 0.2$ , and `tilt up/down` based on the sign of  $\Delta_{\text{tilt}}$  when  $\Sigma_{\text{tilt}} > 0.2$ .

**Translation-dominant case.** If translation is significant, we compute the net translation in the initial camera frame:

$$\Delta \mathbf{t}_{\text{cam}} = \mathbf{R}_1^\top (\mathbf{t}_T - \mathbf{t}_1),$$

with components  $(x, y, z)$  corresponding to forward, lateral, and vertical motion, respectively. We use an adaptive threshold  $t_{\text{move}} = \max(0.3 \cdot \|\Delta \mathbf{t}_{\text{cam}}\|_\infty, 0.5)$  to decide whether a component is dominant.

To distinguish `arc` from near-straight translation, we estimate path curvature

$$\kappa = \frac{\sum_t \|\mathbf{f}_t - \mathbf{f}_{t-1}\|_2}{\sum_t \|\mathbf{t}_t - \mathbf{t}_{t-1}\|_2 + \epsilon},$$

where  $\mathbf{f}_t$  is the camera forward vector in world coordinates. If  $\kappa > 9 \times 10^{-4}$ , we classify the segment as `arc cw/ccw` based on the sign of  $\Delta_{\text{pan}}$ , and optionally add auxiliary

Table 1. **Atomic camera motion primitives.** We list the  $K=15$  primitives used in our benchmark, grouped by geometric degree of freedom (rotations, translations, coupled motion, and static). Opposing directions within each axis are mutually exclusive, forming the basis of our incompatibility constraints, while primitives across different axes may co-occur under a constrained multi-label formulation.

Axis	Primitive	Operational Definition	Mutual exclusion
Yaw	pan left / pan right	Horizontal rotation about vertical axis	pan left $\leftrightarrow$ pan right
Pitch	tilt up / tilt down	Vertical rotation about horizontal axis	tilt up $\leftrightarrow$ tilt down
Roll	roll cw / roll ccw	In-plane rotation about optical axis	roll cw $\leftrightarrow$ roll ccw
Y	truck left / truck right	Lateral translation parallel to image plane	truck left $\leftrightarrow$ truck right
Z	crane up / crane down	Vertical translation of camera center	crane up $\leftrightarrow$ crane down
X	dolly in / dolly out	Translation along view axis	dolly in $\leftrightarrow$ dolly out
Coupled	arc cw / arc ccw	Coupled yaw + lateral translation	arc cw $\leftrightarrow$ arc ccw
None	static	No dominant motion above thresholds	static $\leftrightarrow$ any non-static

Table 2. Positioning of CameraMotionDataset and CameraMotionVQA against related benchmarks and cinematic datasets. We contrast task focus, temporal unit, label structure (including whether explicit constraints or QA protocols are provided), camera-motion granularity, intended use, and whether explicit camera parameters (geometry access) are available.

Work	Primary focus	Temporal unit	Label type (constraints / QA)	Motion granularity	Intended use	Geometry access
CameraBench [1]	Camera motion primitives in diverse real-world videos; taxonomy + label-then-caption annotations.	Short video clips (avg. ~5–6s); shot-aligned / manually segmented.	Multi-label binary primitive tags (~50); plus captions and paired yes/no VQA skill probes.	Primitive-level; directional primitives (translation / rotation / zoom / tracking, etc.).	Mixed: benchmark suite (classification, retrieval, captioning, VQA) + small-scale training for motion-aware VLMs.	<b>No:</b> real videos (no ground-truth camera parameters).
CineTechBench [4]	Broad cinematographic techniques (scale, angle, composition, movement, lighting, color, focal length) with expert annotation.	Movie images + short movie clips/shots (~600 images, 120 clips).	Manual technique labels; question-answer pairs and annotated descriptions for understanding; separate camera-movement generation evaluation.	Coarse-to-mid: technique categories; camera movement is one dimension among 7.	Diagnostic benchmark (understanding + generation evaluation).	<b>No:</b> no explicit camera parameters provided.
VidComposition [3]	Composition understanding in compiled videos (cinematography, character, narrative, scene, making).	Compiled videos (avg. ~20 min) segmented into coherent sections.	Human-annotated multiple-choice QA (982 videos / 1706 questions) across 15 sub-tasks, including camera movement / angle / shot size perception.	Coarse-to-mid: composition attributes; camera motion appears as a perceptual attribute in QA.	Diagnostic benchmark for MLLMs on compiled-video composition.	<b>No:</b> no explicit camera parameters provided.
CineScale2 [2]	Cinematic camera features (camera angle + camera level) on movie frames/images.	Frames / images (~24.7k).	Single-label categorical annotations per attribute (angle: 5 classes; level: 6 classes).	<i>N/A for motion</i> (static camera setup attributes only).	Training-scale dataset for recognition of camera angle/level; film-style analysis.	<b>No:</b> no explicit camera parameters provided.
<b>CameraMotionDataset</b>	Camera motion primitive dataset for controlled supervision and motion-token distillation.	<b>Within-shot 1s segments</b> (fixed-length; shot-consistent).	<b>Constrained multi-label</b> primitive annotations with axis-wise incompatibility constraints.	<b>Primitive-level; directional; axis-wise constraints;</b> supports compound motions within 1s.	<b>Supervision dataset</b> (training / distillation / controlled analysis).	<b>Yes:</b> synthetic camera parameters available (controlled rendering).
<b>CameraMotionVQA</b>	Camera-motion sensitivity benchmark for VideoLLM evaluation via structured prompting.	Same 1s within-shot segments mapped to QA format.	<b>Standardized multiple-choice VQA protocol</b> derived from ground-truth primitives; constraint-consistent answer space.	Primitive-level reasoning over directional motions (single and compound).	<b>Diagnostic benchmark</b> for motion-aware understanding and prompting.	Implicit (inherits synthetic geometry from CameraMotionDataset; not directly exposed to models).

tilt or dolly if their corresponding rotation/translation magnitudes exceed thresholds. Otherwise, we assign axis-aligned translation primitives according to dominant components: dolly in/out from  $x$ , truck left/right from  $y$ , and crane up/down from  $z$ .

**Roll.** We additionally assign roll cw/ccw only when for-

ward motion is present and  $\Sigma_{\text{roll}} > 0.5$ , which avoids spurious roll labels from minor numerical jitter.

To verify the correctness of the automatic mapping, we randomly sampled 720 segments and collected primitive annotations using the same 15-label set. Annotators were instructed to select the correct option from an MCQ-style

---

**Algorithm 1** Pose-to-label mapping

---

**Require:** Extrinsics  $\{(\mathbf{R}_t, \mathbf{t}_t)\}_{t=1}^T$

- 1:  $\mathcal{Y} \leftarrow \emptyset$
- 2: Compute  $d_{\text{trans}}$  (total translation distance) and  $(\Delta_{\text{pan}}, \Delta_{\text{tilt}})$ ,  $(\Sigma_{\text{pan}}, \Sigma_{\text{tilt}})$  (signed / abs rotation stats)
- 3: **if**  $d_{\text{trans}} < 0.05$  **then** ▷ rotation-dominant / static
- 4:   **if**  $\Sigma_{\text{pan}} < 0.2$  **and**  $\Sigma_{\text{tilt}} < 0.2$  **then**
- 5:     **return** {static}
- 6:   **end if**
- 7:   **if**  $\Sigma_{\text{pan}} > 0.2$  **then**
- 8:      $\mathcal{Y} \leftarrow \mathcal{Y} \cup \{\text{pan right}\}$  **if**  $\Delta_{\text{pan}} > 0$  **else**  $\mathcal{Y} \leftarrow \mathcal{Y} \cup \{\text{pan left}\}$
- 9:   **end if**
- 10:   **if**  $\Sigma_{\text{tilt}} > 0.2$  **then**
- 11:      $\mathcal{Y} \leftarrow \mathcal{Y} \cup \{\text{tilt down}\}$  **if**  $\Delta_{\text{tilt}} > 0$  **else**  $\mathcal{Y} \leftarrow \mathcal{Y} \cup \{\text{tilt up}\}$
- 12:   **end if**
- 13: **else** ▷ translation-dominant
- 14:   Compute  $\Delta \mathbf{t}_{\text{cam}}$  and  $t_{\text{move}}$
- 15:   Compute curvature  $\kappa$  from forward vectors
- 16:   **if**  $\kappa > 9 \times 10^{-4}$  **then**
- 17:      $\mathcal{Y} \leftarrow \mathcal{Y} \cup \{\text{arc cw}\}$  **if**  $\Delta_{\text{pan}} > 0$  **else**  $\mathcal{Y} \leftarrow \mathcal{Y} \cup \{\text{arc ccw}\}$
- 18:   **end if**
- 19:   Update  $\mathcal{Y}$  with dolly in/out (forward-dominant), truck left/right (lateral-dominant), and crane up/down (vertical-dominant)
- 20: **end if**
- 21: **return** Canonicalize( $\mathcal{Y}$ ) (Sec. A.2)

---

VQA benchmark and to prioritize dominant motion over minor jitter. The resulting agreement accuracy is 93%, supporting the reliability of the pose-to-label mapping procedure.

## B.2. Re-balancing and class distribution

The full pose-to-label conversion over all rendered videos produces 542,504 1-second segments. As shown in Fig. 2(a), due to the scripted camera trajectories in the synthetic generator, the resulting label distribution is highly imbalanced. In particular, simple directional primitives such as `tilt down` and `arc ccw` occur far more frequently than rarer motions such as `roll cw/ccw`. Without re-balancing, this imbalance would bias classifiers toward dominant primitives and obscure diagnostic conclusions about motion sensitivity in VideoLLMs.

To mitigate this effect, we apply per-label-set downsampling. For each unique canonical label set (Sec. A.2) (e.g., `tilt up` and `pan left`), we cap the number of segments to at most 200 samples. If a label set contains fewer than 200 segments, all instances are retained. This strategy preserves the diversity of primitive combinations while preventing over-representation of frequent motion patterns.

After re-balancing, the final dataset contains **12,274** segments. Figure 2 visualizes the label-set frequency distribution before and after downsampling. The post-balanced distribution is substantially flatter, enabling more controlled evaluation of primitive-level recognition and structured

prompting.

## C. CameraMotionVQA Protocol

### C.1. Prompt templates and answer normalization

Each 1-second clip in CameraMotionDataset is converted into a 4-way multiple-choice VQA instance by pairing the video with a fixed prompt template and four candidate label sets (one correct and three distractors). We use the following prompt string (shown verbatim) with lettered options:

```
<video>
Identify the camera motion depicted in
the video using standard cinematographic
terminology.
Options:
(A) <optA>
(B) <optB>
(C) <optC>
(D) <optD>
```

The reference answer is stored as `Answer: <letter>`.

**Option text.** For readability, we verbalize `cw/ccw` as `clockwise/counterclockwise` in options, while preserving all other primitive names (e.g., `pan left`, `dolly in`). Multi-primitive options are formatted as a comma-separated list in canonical order (Sec. A.2).

**Answer parsing.** At evaluation time, we normalize model outputs by extracting the first occurrence of a valid choice letter in  $\{A,B,C,D\}$  (case-insensitive), optionally preceded by the token `Answer:`. If no valid letter is found, model output will be parsed to try to match the ground truth; otherwise, the prediction is marked as invalid. This normalization ensures a consistent, model-agnostic scoring interface for VideoLLMs.

### C.2. Distractor sampling algorithm

As shown in Algorithm 2, a naïve distractor strategy (sampling arbitrary label sets) can make questions either trivial (e.g., mismatched label cardinality) or invalid (e.g., violating incompatibility constraints). We therefore sample distractors from a precomputed pool  $\mathcal{Y}$  of *canonicalized, constraint-valid* label sets (Sec. A.2), stratified by label cardinality  $c \in \{1, 2, 3\}$ .

**Complexity-matched distractors.** Given a ground-truth label set  $y^*$  with complexity  $c = |y^*|$ , we sample distractors using the following rule, matching the implementation in our dataset generator:

- If  $c = 1$ : sample 3 distractors from single-label sets and 1 distractor from two-label sets.
- If  $c = 2$ : sample 2 distractors from two-label sets, 1 from single-label sets, and 1 from three-label sets.

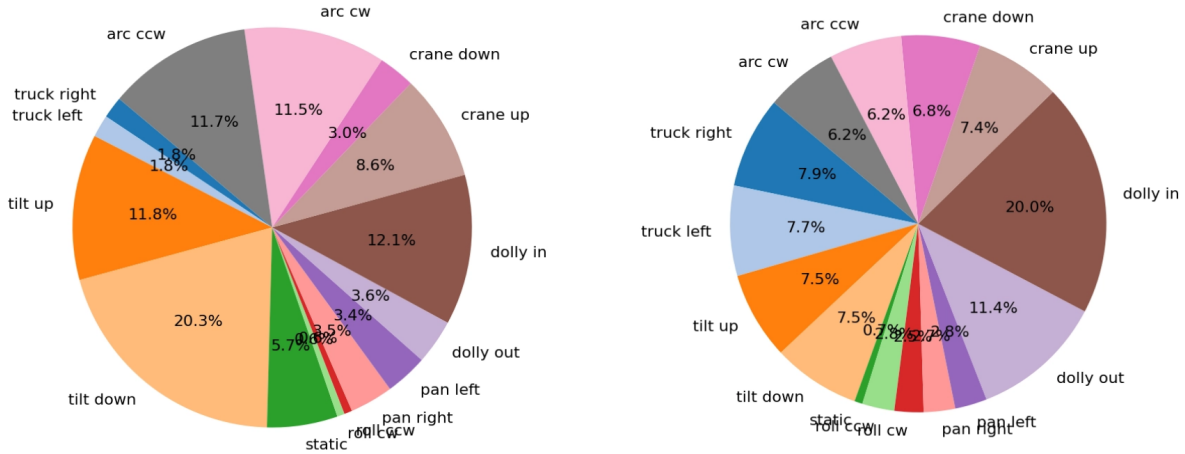


Figure 2. **Label-set distribution before and after re-balancing.** We cap each canonical primitive combination at 200 segments. The original distribution is highly skewed toward common directional motions, while the rebalanced dataset provides a more uniform coverage across primitive combinations.

**Algorithm 2** Distractor sampling for CameraMotionVQA (4-way MCQ)

**Require:** GT label set  $y^*$ ; pools  $\mathcal{Y}_1, \mathcal{Y}_2, \mathcal{Y}_3$  of valid label sets with  $|y| = 1, 2, 3$

- 1:  $c \leftarrow |y^*|$ ;  $\mathcal{O} \leftarrow \emptyset$
- 2: **if**  $c = 1$  **then**
- 3:    $\mathcal{O} \leftarrow \text{Sample}(\mathcal{Y}_2, 1) \cup \text{Sample}(\mathcal{Y}_1, 3)$
- 4: **else if**  $c = 2$  **then**
- 5:    $\mathcal{O} \leftarrow \text{Sample}(\mathcal{Y}_1, 1) \cup \text{Sample}(\mathcal{Y}_3, 1) \cup \text{Sample}(\mathcal{Y}_2, 2)$
- 6: **else**
- 7:    $\mathcal{O} \leftarrow \text{Sample}(\mathcal{Y}_2, 2) \cup \text{Sample}(\mathcal{Y}_3, 1)$
- 8: **end if**
- 9: Replace one element in  $\mathcal{O}$  with  $y^*$  to ensure exactly one correct option
- 10: Verbalize  $cw/ccw \rightarrow \text{clockwise/counterclockwise}$ ; shuffle and assign letters A–D
- 11: **return** Options  $\{(A, y_A), (B, y_B), (C, y_C), (D, y_D)\}$  and correct letter

- If  $c = 3$ : sample 2 distractors from two-label sets and 1 from three-label sets (then insert  $y^*$  to ensure one correct option).

This yields a mixture of easy and moderately hard negatives while avoiding degenerate cases where the correct answer is identifiable solely by the number of primitives.

**Constraint validity.** All candidates (including distractors) are drawn from  $\mathcal{Y}$ , which contains only incompatibility-consistent label sets. As a result, every option is valid under the same constraint system as the ground truth, preventing models from exploiting constraint violations as shortcuts.

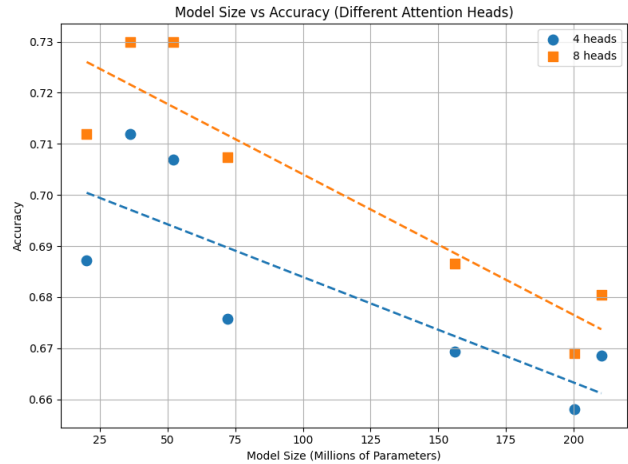


Figure 3. **Classifier capacity ablation.** Accuracy versus classifier size (M parameters) for varying Transformer depth, head count, and hidden dimension. Overall performance saturates with small models; using 8 attention heads yields a modest but consistent gain over 4 heads.

**D. Additional Experimental Results**

**D.1. Classifier capacity ablation**

We study the effect of classifier capacity on camera-motion recognition. The classifier is a lightweight Transformer encoder operating on frozen VideoLLM vision features. We vary three architectural parameters: the number of encoder blocks (2–6), the number of attention heads (4 or 8), and the hidden dimension (256–896).

Figure 3 plots accuracy as a function of model size. Across all configurations, performance varies within a rel-

atively narrow range (about 0.71–0.79), indicating that increased classifier capacity does not consistently translate to higher accuracy. The best results are obtained with small models (20–50M parameters), while larger configurations with wider hidden dimensions or additional layers do not provide reliable improvements.

Increasing the number of attention heads yields a modest gain (typically 1–2%), but the overall trend shows early saturation: models larger than roughly 50M parameters do not improve performance and sometimes degrade slightly. This behavior is consistent with a representation bottleneck in the frozen vision features, but it may also reflect limited supervision after re-balancing (Sec. B.2), where the effective training set size is relatively small for fitting larger classifiers. A potential direction to better exploit higher-capacity heads is to increase data diversity via augmentation, *e.g.*, temporal replay/resampling within the 1-second clip, synthetic camera roll perturbations, and scale-preserving random crops (to simulate focal-length and framing variation) while keeping the motion label unchanged.

## D.2. Per-label breakdown and confusion analysis

We provide per-label analysis for the three camera-motion recognition pipelines used throughout the paper: *VGGT classifier* (teacher cues), *VGGT-Q-Former* (distilled student cues), and *Q-Former probing* (diagnostic baseline on frozen VideoLLM vision features). Following Tab. 2 in the main paper, we report class-averaged and frequency-weighted scores: the overall **Macro-F1 / Weighted-F1** are **0.87 / 0.92** (VGGT classifier), **0.83 / 0.87** (VGGT-Q-Former), and **0.69 / 0.74** (Q-Former probing). These aggregate gaps are reflected consistently in the per-primitive results in Tab. 3.

**Per-label breakdown.** Tab. 3 reports F1 for each primitive. VGGT-derived cues yield uniformly strong performance across most translation and rotation primitives, with several classes exceeding 0.9 F1 (*e.g.*, *dolly in/out*, *crane up/down*, *truck left/right*, *roll cw*). Distilling VGGT cues into a compact Q-Former incurs a moderate but systematic drop (typically 0.03–0.06 F1 per class), while still substantially outperforming probing. This aligns with the intended accuracy–throughput trade-off: the VGGT classifier achieves the best recognition accuracy but requires running the 3D backbone, whereas VGGT-Q-Former reuses frozen VideoLLM visual features at inference time and is therefore significantly more efficient.

The most challenging class is *static*, which has the lowest F1 across all methods. This is expected because *static* is defined by the *absence* of dominant motion above thresholds, and minor camera jitter or object-induced apparent motion can easily trigger false positives. Similarly, *pan* and *tilt* are moderately harder than most translation primitives, as they are more easily confounded with arc-like

Table 3. **Per-primitive F1 scores.** VGGT classifier achieves the best accuracy and consistently outperform the other two methods. A similar trend is visible between VGGT-Q-Former and Q-Former probing. However, the VGGT classifier requires running the 3D backbone, leading to higher computational and memory overhead. VGGT-Q-Former reuses frozen VideoLLM vision features and trades a modest accuracy drop for substantially higher throughput. Compared to probing, both VGGT-derived variants improve nearly all primitives, with the largest gains on ambiguous motions (*pan*, *tilt*) and the *static* class.

Primitive	VGGT Classifier	VGGT-Q-Former	Q-Former Probing
arc ccw	0.88	0.83	0.68
arc cw	0.94	0.90	0.75
crane down	0.94	0.89	0.74
crane up	0.93	0.88	0.72
dolly in	0.94	0.90	0.78
dolly out	0.90	0.85	0.75
pan left	0.83	0.76	0.58
pan right	0.85	0.80	0.66
roll ccw	0.91	0.86	0.71
roll cw	0.97	0.92	0.83
static	0.65	0.44	0.27
tilt down	0.94	0.90	0.78
tilt up	0.89	0.83	0.69
truck left	0.93	0.88	0.74
truck right	0.92	0.88	0.77
<b>Macro F1</b>	<b>0.87</b>	<b>0.83</b>	<b>0.69</b>

camera paths and with subtle changes in viewpoint.

**Confusion analysis.** Figure 4 reveals that residual errors of the VGGT classifier are *highly structured* and dominated by a few recurring confusion patterns rather than broadly distributed noise.

First, there is a pronounced tendency to over-predict *dolly out* as a false positive across multiple ground-truth classes: both *crane up* and *crane down* are frequently mislabeled as *dolly out* (*e.g.*, 15 and 9 counts, respectively), and similarly for *truck left/right* (11 counts each) and *tilt up/down* (8–7 counts). This suggests that, in some segments, outward depth change acts as an “attractor” class, likely because multiple camera trajectories contain a depth component and the mapping reduces a continuous pose trajectory to discrete primitives.

Second, we observe systematic confusions among coupled motions and axis-aligned primitives. In particular, *arc cw/ccw* is often confused with *dolly out* and with horizontal motion primitives (*e.g.*, *pan right*), consistent with the fact that *arc* combines yaw rotation with lateral translation and may also include a depth component depending on the trajectory. For example, *arc cw* is frequently predicted as *dolly out* or *pan right*, while *arc ccw* shows con-

fusion with `truck right` and `dolly out`.

Third, the largest single off-diagonal entry corresponds to `dolly in` being misclassified as `pan right` (16 counts), indicating that certain trajectories exhibit concurrent yaw change and forward motion where the dominant primitive is ambiguous at 1-second granularity. Similar interactions appear between `tilt` and translation primitives, where pitch changes co-occur with camera motion and lead to mixed predictions.

Finally, `static` errors are sparse but concentrated: when misclassified, `static` is most often predicted as `dolly out` (3 counts), consistent with threshold-boundary cases where small residual translation exceeds the “no dominant motion” criterion.

Overall, the confusion matrix indicates that the remaining failure modes are driven primarily by (i) discretization of continuous camera trajectories into primitives and (ii) co-occurring multi-axis motions where one component (notably depth change) is over-selected. This motivates both the constrained multi-label formulation (to allow co-occurrence) and future improvements in pose-to-label mapping (e.g., better dominance criteria for separating depth change from vertical/lateral translation in short clips).

## E. Full Prompts and additional Qualitative Examples

### E.1. Full prompt templates

We evaluate how explicit camera-motion cues affect *VideoLLM* generation using three prompts that share the same video input (a sequence of uniformly sampled frames) and differ only in whether and how motion information is communicated. The *motion-header prompt* follows the structured prompting design in the main paper (Sec. 3.5), where a per-second motion list is prepended as a compact textual scaffold [1].

**Baseline prompt (generic description).** This is the default VideoLLM usage pattern: the model receives frames and a generic captioning instruction, without any explicit cinematography cues.

```
Here are [N] consecutive video frames.
They are evenly sampled at a frame rate
of [r] FPS.
```

```
Describe the video clip using clear and
concise language. Make your description
in one paragraph.
```

In practice, this prompt often yields content-correct but camera-vague descriptions, and may conflate camera motion with object motion.

**Structured prompt (filmmaker-style instruction).** Motivated by the qualitative prompting protocol, we reformulate the instruction in filmmaking language to explicitly request

cinematographic attributes (lighting, framing, composition) and to encourage temporal linking across frames.

```
Here are [N] consecutive video frames.
They are evenly sampled at a frame rate
of [r] FPS.
```

```
Describe this video using the filmmaker's
language, highlighting the lighting,
framing, video composition, and
especially camera usage that connects
different frames. For example: ``At the
beginning, <video content>; then <camera
motion>, <video content>; ...; finally,
<camera motion>, <video content>``. Make
your description in a paragraph.
```

This structure improves the *intent* to discuss camera usage, but it still requires the VideoLLM to infer motion direction and temporal evolution solely from its visual representation. **Camera motion injected structured prompt.** We inject predicted motion primitives as a short header before the same filmmaker-style instruction. Following Sec. 3.5 of the main paper, a shot with  $S$  one-second segments is serialized as a list Per-second camera motion:  $[m_1, \dots, m_S]$ , where each  $m_s$  is a canonicalized set of primitives (e.g., `static` or `pan left + tilt up`).

```
Here are [N] consecutive video frames.
They are evenly sampled at a frame rate
of [r] FPS.
```

```
Per-second camera motion: [m1, m2, ...,
mS].
```

```
Describe this video using the filmmaker's
language, highlighting the lighting,
framing, video composition, and
especially camera usage that connects
different frames. For example: ``At the
beginning, <video content>; then <camera
motion>, <video content>; ...; finally,
<camera motion>, <video content>``. Make
your description in a paragraph.
```

This modification is *training-free*: it does not change VideoLLM weights or architecture, but conditions generation on an explicit motion prior.

We design the motion header to be *compact*, *structured*, and *physically grounded* (primitive taxonomy with constraints). This choice is motivated by two empirical observations. First, probing shows that camera motion is only weakly recoverable from frozen VideoLLM vision features, making direction and temporal consistency brittle without additional cues. Second, camera motion is intrinsically compositional and time-indexed; a per-second list matches the segment granularity of our benchmark and provides a stable alignment target for the language model. As discussed in the main paper, providing explicit per-second motion labels encourages temporally grounded narratives, reduces motion-direction hallucinations, and biases the model toward continuity-aware reasoning (e.g., linking

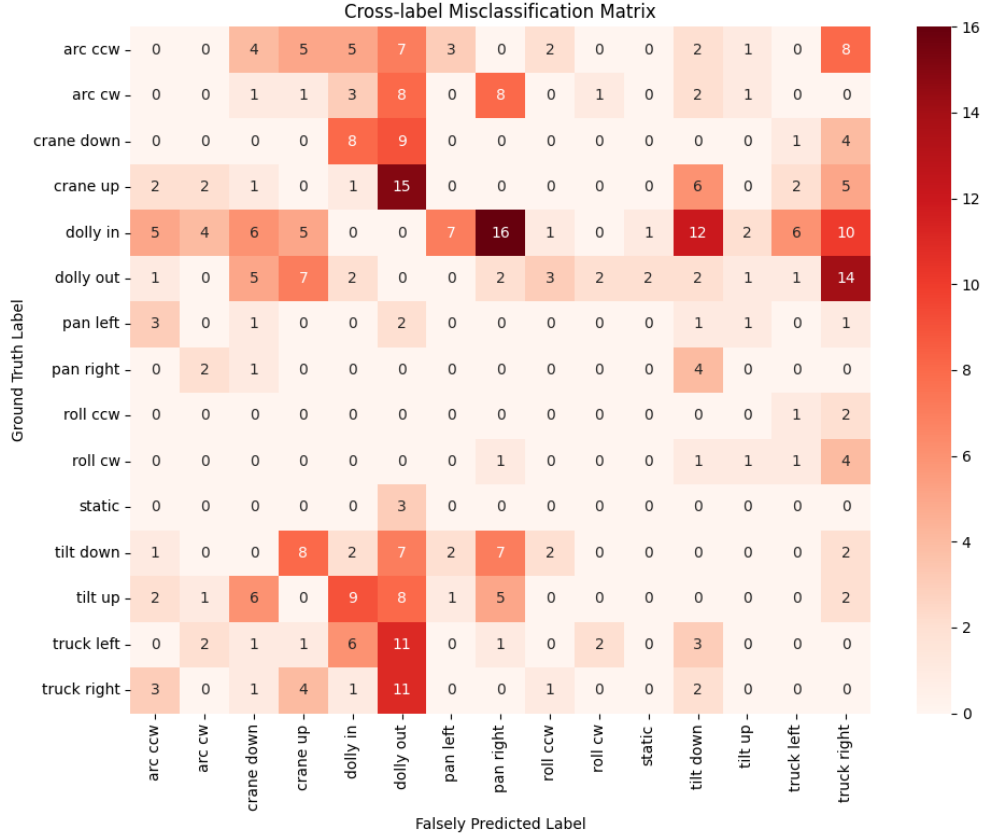


Figure 4. **Cross-label confusion for the VGGT classifier.** Rows denote ground-truth primitives and columns denote falsely predicted primitives (higher intensity indicates more frequent confusion). The label order matches Tab. 3 and the dataset primitive indices.

subject changes to camera transitions) rather than producing generic cinematography statements.

## E.2. More qualitative examples

To further illustrate the effect of camera-motion prompting, we provide additional qualitative examples from *CineTech-Bench* [4]. For each clip, we compare the outputs produced by the three prompt variants described in Sec. E.1: *baseline*, *structured*, and our *motion-header* prompt.

Figures 5 (Clip2) and 6 (Clip3) show sampled frames from two example clips. Together with the example shown in the main paper (Clip1), we present three representative cases covering different camera motions and scene types. For each clip, we report the generated descriptions under the three prompt settings, resulting in nine outputs in total (Tab. 4, 5, 6). Key phrases related to camera motion are highlighted for comparison.

Across the three examples, the baseline prompt primarily focuses on scene content and rarely provides reliable descriptions of camera motion. The structured prompt encourages the model to discuss cinematographic aspects, but the inferred motion cues are often ambiguous or incorrect.

For instance, in Clip1, the structured prompt incorrectly describes the motion as a *whip pan to the right*, while the injected motion header leads the model to correctly describe alternating *pan-left* and *pan-right* movements that match the camera dynamics. In Clip2, the structured prompt identifies a rolling camera but does not clearly specify its direction or temporal progression, whereas the motion-header prompt explicitly grounds the description in a *clockwise roll* combined with *trucking* and *dolly-out* movements, producing a more precise and temporally coherent narrative. In Clip3, the structured prompt relies on loosely defined cinematographic terms such as “push-in” or “tracking forward,” which describe similar motion but lack a consistent taxonomy and omit the camera roll entirely. In contrast, the motion-header prompt enforces explicit primitives such as *dolly-in* and *roll clockwise*, yielding a more unified and geometrically grounded description. These examples highlight that while structured prompting alone encourages camera-aware language, providing explicit motion primitives substantially improves directional correctness, terminological consistency, and temporal grounding in VideoLLM-generated descriptions.



Figure 5. Clip2 sampled frames from CineTechBench [4].

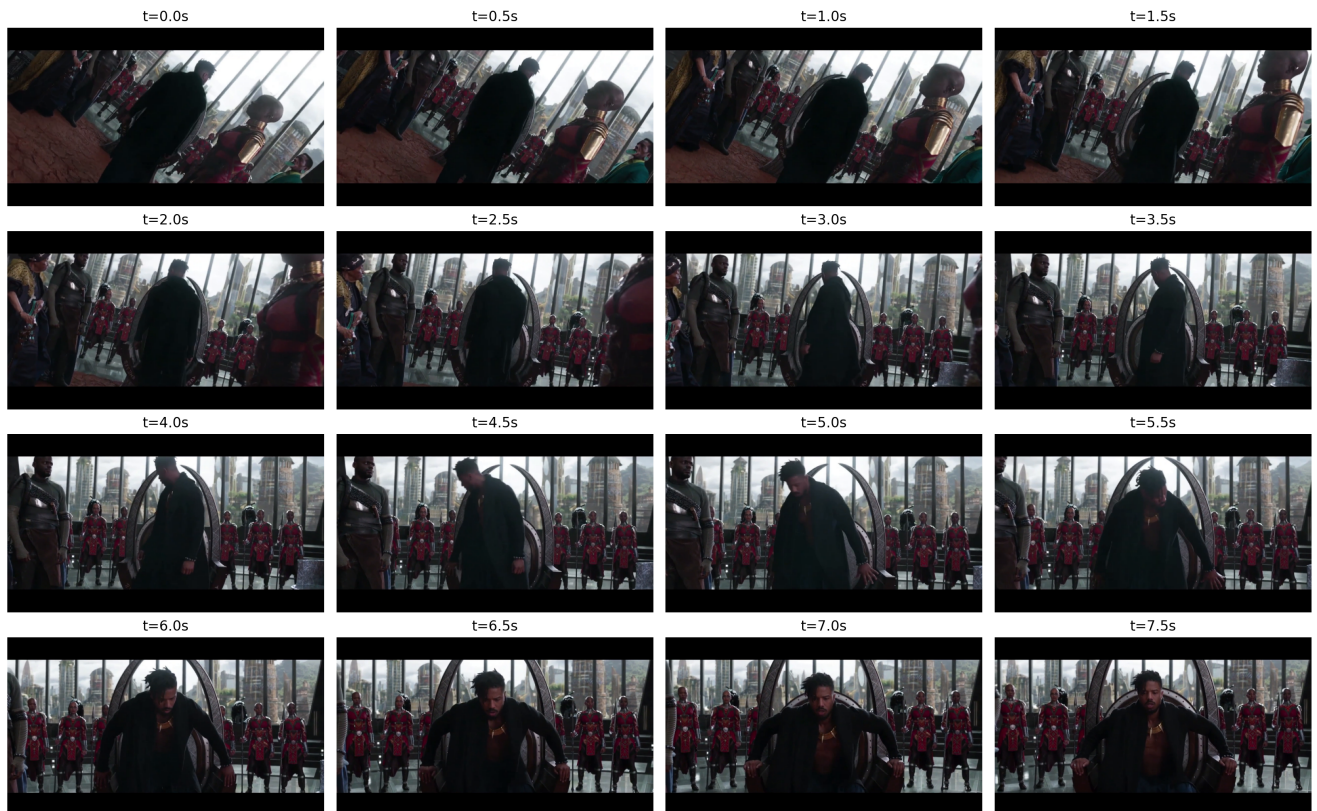


Figure 6. Clip3 sampled frames from CineTechBench [4].

Table 4. Qualitative comparison of model-generated descriptions for Clip1 under different prompt templates. Camera motion-related phrases are highlighted in bold.

Baseline prompt	Structured prompt (filmmaker-style instruction)	Camera motion injected structured prompt
<p>This video portrays a dramatic musical performance scene. It begins with a conductor, dressed in black, gesturing with precision and intensity, likely cueing the start of a musical piece. His facial expression is focused and assertive, signaling a moment of high tension. The camera quickly <b>pans</b> with <b>motion blur</b>, transitioning to a drummer mid-performance, energetically striking the drums while accompanied by a bassist. The <b>motion blur</b> appears again between frame changes, emphasizing swift <b>camera movement</b> or <b>cuts</b> to maintain rhythmic pacing. The conductor reappears in subsequent frames, continuing to direct with expressive hand movements, culminating in another quick <b>blur</b> before returning to the drummer, now deeply immersed in an intense and possibly climactic moment. The alternating shots and dynamic movement suggest a tightly <b>edited sequence</b> synchronized with musical tempo, evoking a sense of urgency and artistic fervor typical of a performance climax.</p>	<p>At the beginning, the video opens with a medium close-up of the conductor, dramatically lit with focused, warm stage lighting that casts soft shadows and isolates him against the dimly lit auditorium, emphasizing his stern facial expression and sharp, deliberate hand gestures. Then, a rapid <b>whip pan to the right</b> (evident from <b>motion blur</b>) bridges the visual transition, dynamically redirecting the viewer's focus to the drummer. The <b>camera settles</b> into a medium-wide shot of the drum set, capturing the drummer mid-performance under similarly warm, directional lighting that accentuates the shimmer of the cymbals and the energy of his movements. The <b>framing</b> includes part of the upright bassist, preserving ensemble context while maintaining the drummer as the focal point. Another <b>whip pan</b> follows, visually echoing the earlier motion and swiftly returning the viewer to the conductor. As the video <b>cuts back</b>, the conductor appears more animated in his movements, with tight <b>framing</b> and consistent lighting maintaining visual continuity. A final <b>whip pan</b> transitions back to the drummer, who now performs with increased intensity, reinforcing the escalating rhythm and emotional tension through repeated visual interplay. The sequence's <b>camera work</b>—marked by fluid <b>whip pans</b>—mirrors the musical tempo, while the lighting and composition maintain dramatic cohesion, heightening the confrontation and synchrony between conductor and performer.</p>	<p>At the beginning, under warm, low-key stage lighting, a <b>static</b> medium closeup <b>frames</b> the conductor from stage right, isolating him against a softly lit auditorium background as he cues the ensemble with precise hand gestures. Then, a <b>pan-left</b> motion bridges the space, transitioning fluidly into a medium shot of the drummer, dynamically lit from above to emphasize the percussive energy and <b>motion blur</b> of his performance. Next, a <b>pan-right</b> swiftly returns the focus to the conductor, capturing his sharp directional cues in a near-symmetrical composition that mirrors the earlier frame, reinforcing continuity through motion. A <b>static shot</b> then <b>holds</b> on the conductor, now mid-gesture, in tighter <b>framing</b> that heightens dramatic tension while maintaining spatial coherence. Finally, a <b>pan-left</b> reintroduces the drummer in a more intensified moment—his kinetic energy visually amplified through rhythmic lighting and a centered composition that anchors the visual climax. The sequence skillfully employs lateral <b>camera movement</b> and repeated <b>framing</b> motifs to synchronize the visual rhythm with the musical performance, creating a cohesive and propulsive cinematic language.</p>

Table 5. Qualitative comparison of model-generated descriptions for Clip2 under different prompt templates. Camera motion-related phrases are highlighted in bold.

Baseline prompt	Structured prompt (filmmaker-style instruction)	Camera motion injected structured prompt
<p>The clip shows a wounded man lying motionless on the forest floor among ferns and leaves, his face bruised and smeared with blood, suggesting he has been injured or unconscious. The <b>camera gradually shifts its framing</b> across the scene, revealing more of his body and the surrounding foliage as his head slowly tilts to the side. After remaining still for several moments, he begins to stir slightly, moving his head and hand as if regaining consciousness. Toward the end of the clip, another person enters from the left side, reaching toward him and leaning over his body, apparently checking on him or attempting to help him while the injured man weakly reacts.</p>	<p>At the beginning, the shot opens in a dim, cool-toned forest, lit by soft bluish ambient light. A tight overhead close-up <b>frames</b> a wounded man lying among ferns and damp leaves, his face near the center while foliage fills the surrounding space. As the sequence progresses, the <b>camera slowly drifts laterally while rolling</b>, shifting the man's face from a frontal view to a slightly oblique angle. The <b>framing gradually widens</b> from a centered close-up to a looser, off-center composition, revealing more of his shoulder and the forest floor. The <b>continuous roll with gentle tracking</b> slides his head toward the lower part of the frame while foliage expands across the upper area, creating a drifting, hovering sensation. Toward the end, the <b>camera dollies slightly outward while maintaining the roll</b>, widening the overhead view as another person enters from the left and leans toward the injured man. The shot settles into a <b>loose overhead two-shot</b>, both figures partially visible among the ferns, with the slow rolling camera motion unifying the sequence into a calm but tense visual moment.</p>	<p>The shot opens in a dim, cool-toned forest with soft bluish lighting. A wounded man lies among ferns and damp leaves, <b>framed in a tight overhead close-up</b> that centers on his face and upper torso. The camera <b>rolls slowly clockwise</b>, keeping the close framing while rotating the horizon so the foliage appears to drift around him, creating a disorienting sense of instability. Midway through, the motion becomes more complex: the camera continues the <b>clockwise roll</b> while <b>tracking left</b> and <b>craning up</b>, gradually widening the view and revealing more of the forest floor. Soon after, the camera maintains the roll and begins a gentle <b>dolly out</b>, expanding the overhead composition. As the frame widens, another figure enters from the left, kneels beside the injured man, and reaches toward him. The shot ends in a wider overhead view, with both figures visible among the ferns as the slow <b>rolling, outward-moving camera</b> connects the sequence into a somber, atmospheric moment.</p>

## References

- [1] Zhiqiu Lin, Siyuan Cen, Daniel Jiang, Jay Karhade, Hewei Wang, Chancharik Mitra, Tiffany Ling, Yuhan

Huang, Sifan Liu, Mingyu Chen, et al. Towards understanding camera motions in any video. *arXiv preprint*

Table 6. Qualitative comparison of model-generated descriptions for Clip3 under different prompt templates. Camera motion-related phrases are highlighted in bold.

Baseline prompt	Structured prompt (filmmaker-style instruction)	Camera motion injected structured prompt
<p>A man wearing a long dark coat walks forward through a grand, modern throne room with floor-to-ceiling windows overlooking a futuristic city. Several guards in coordinated red uniforms stand symmetrically on both sides of the room, holding spears and watching as he approaches a large, curved ceremonial throne positioned at the center. Other armored attendants and officials stand nearby, observing quietly. The man slows as he reaches the throne, turns slightly, then lowers himself into the seat, gripping the armrests and settling into a commanding posture while the guards remain lined up behind him, reinforcing the formal and authoritative atmosphere of the scene.</p>	<p>At the beginning, a slightly <b>canted</b> medium-wide establishing shot inside a grand, glass-walled hall, where bright natural daylight floods in from the floor-to-ceiling windows behind the characters, producing strong backlighting and soft silhouettes. In the foreground, a man in a long dark coat walks toward a large circular throne-like structure positioned at the center of the frame, while symmetrical rows of red-armored guards stand rigidly in the background, forming a visual corridor that guides the viewer’s eye inward. As the shot progresses, the <b>camera slowly tracks forward</b> behind him, gradually straightening its angle and <b>tightening the framing</b>, turning the initial off-axis composition into a more centered, ceremonial perspective. The circular throne becomes a dominant compositional element, <b>framing</b> the character as he approaches; the guards remain evenly spaced on both sides, reinforcing the symmetry and depth of the mise-en-scène. Continuing the forward <b>push-in</b>, the camera subtly <b>lowers and stabilizes into a frontal alignment</b> as the man reaches the throne, placing him precisely on the central axis of the architecture and the guard formation. He then turns and lowers himself into the seat, the movement captured in a steady medium shot that emphasizes the ritualistic nature of the action. Finally, as he settles into the throne and grips the armrests, the camera completes its <b>push-in</b> to a centered, balanced composition: the character sits framed by the curved throne behind him, flanked symmetrically by the guards and the luminous cityscape beyond the windows, creating a powerful throne-room tableau under strong backlighting.</p>	<p>At the beginning, a slightly <b>canted wide shot</b> reveals a grand, glass-walled hall flooded with soft daylight from floor-to-ceiling windows, the bright skyline forming a luminous backdrop while a group of red-armored guards stands in symmetrical formation. A man in a dark coat walks toward a sculptural throne framed by two curved metallic blades. As the camera <b>dollies in while rolling clockwise</b>, the off-axis framing creates a subtle sense of motion and tension, gradually tightening the composition around the man’s back and the throne. The <b>dolly-in with clockwise roll continues</b>, bringing the throne into clearer alignment behind him while the guards remain evenly spaced on both sides, their red armor catching rim light from the windows. The lighting stays high-key and backlit, outlining figures with soft highlights while the foreground remains slightly shadowed, adding depth. As the camera <b>keeps dollaying in and rolling clockwise</b>, the frame slowly levels and the throne becomes centered in the composition. The man turns and lowers himself toward the seat, the curved blades of the throne visually framing his body. Finally, the <b>dolly-in with clockwise roll resolves into a centered medium shot</b>, where he settles into the throne and grips the armrests, with the guards standing symmetrically behind him and the bright cityscape still glowing through the windows, completing the camera’s smooth approach and stabilizing the composition around his newly assumed position of authority.</p>

*arXiv:2504.15376*, 2025. 1, 3, 7

- [2] Mattia Savardi, András Bálint Kovács, Alberto Signoroni, and Sergio Benini. Cinescale2: a dataset of cinematic camera features in movies. *Data in Brief*, 51:109627, 2023. 3
- [3] Yunlong Tang, Junjia Guo, Hang Hua, Susan Liang, Mingqian Feng, Xinyang Li, Rui Mao, Chao Huang, Jing Bi, Zeliang Zhang, et al. Vidcomposition: Can mllms analyze compositions in compiled videos? In *CVPR*, pages 8490–8500, 2025. 3
- [4] Xinran Wang, Songyu Xu, Xiangxuan Shan, Yuxuan Zhang, Muxi Diao, Xueyan Duan, Yanhua Huang, Kongming Liang, and Zhanyu Ma. Cinetechbench: A benchmark for cinematographic technique understanding and generation. *arXiv preprint arXiv:2505.15145*, 2025. 3, 8, 9